

1 **Nicotinic acetylcholine receptor signaling maintains epithelial barrier**
2 **integrity**

3

4 Nadja S. Katheder¹, Kristen C. Browder¹, Diana Chang², Ann De Mazière³, Pekka Kujala³,
5 Suzanne van Dijk³, Judith Klumperman³, Zijuan Lai⁴, Dewakar Sangaraju⁴, Heinrich
6 Jasper^{1*}

7

8 ¹Regenerative Medicine, Genentech, South San Francisco, United States

9 ²Human Genetics, Genentech, South San Francisco, United States

10 ³Center for Molecular Medicine, Cell Biology, University Medical Center Utrecht, The
11 Netherlands

12 ⁴Drug Metabolism & Pharmacokinetics, Genentech, South San Francisco, United
13 States

14

15 * corresponding author: jasperh@gene.com

16

17

18

19 **Abstract**

20 **Disruption of epithelial barriers is a common disease manifestation in chronic**
21 **degenerative diseases of the airways, lung and intestine. Extensive human genetic**
22 **studies have identified risk loci in such diseases, including in chronic obstructive**
23 **pulmonary disease (COPD) and inflammatory bowel diseases (IBD). The genes**
24 **associated with these loci have not fully been determined, and functional**
25 **characterization of such genes requires extensive studies in model organisms.**
26 **Here, we report the results of a screen in *Drosophila melanogaster* that allowed for**
27 **rapid identification, validation and prioritization of COPD risk genes that were**
28 **selected based on risk loci identified in human genome-wide association studies**
29 **(GWAS) studies. Using intestinal barrier dysfunction in flies as a readout, our**
30 **results validate the impact of candidate gene perturbations on epithelial barrier**

31 **function in 56% of the cases, resulting in a prioritized target gene list. We further**
32 **report the functional characterization in flies of one family of these genes,**
33 **encoding for nicotinic acetylcholine receptor subunits (nAChR). We find that**
34 **nAChR signaling in enterocytes of the fly gut promotes epithelial barrier function**
35 **and epithelial homeostasis by regulating the production of the peritrophic matrix.**
36 **Our findings identify COPD associated genes critical for epithelial barrier**
37 **maintenance, and provide insight into the role of epithelial nAChR signaling for**
38 **homeostasis.**

39

40 **Introduction**

41 Barrier epithelia such as the skin, linings of the gastrointestinal and urogenital tracts and
42 the airways play a critical role in maintaining a strict separation of external and internal
43 environments, yet also enable the exchange of gases, water, nutrients and immune
44 mediators. They serve as a first layer of defense against external insults and possess
45 remarkable regenerative capacity that declines with age (Jasper, 2020). In *Drosophila*,
46 loss of intestinal barrier function is accompanied by commensal dysbiosis and
47 inflammation and reliably predicts impending organismal death (Rera et al., 2012).
48 Similarly, increased barrier permeability and changes in microbiome composition and
49 abundance have been reported in various human diseases, such as inflammatory bowel
50 disease and chronic obstructive pulmonary disease (COPD) (Raftery et al., 2020).

51 COPD is a major contributor to global morbidity and mortality and is characterized by an
52 obstructed airflow resulting in shortness of breath upon exertion. At the tissue level, lungs
53 of COPD patients display chronic inflammation, extensive cellular remodeling and barrier
54 dysfunction (Aghapour et al., 2018; Barnes, 2019; Carlier et al., 2021).

55 While smoking or exposure to environmental air pollutants remain major risk factors,
56 many COPD patients are non-smokers, suggesting a genetic component contributing to
57 disease susceptibility (Aghapour et al., 2022; Barnes, 2019). Several GWAS studies have
58 been performed in which risk loci for incidence of COPD have been identified (Hobbs et
59 al., 2017; Pillai et al., 2009; Sakornsakolpat et al., 2019). One of the most well-known risk
60 loci is located near the nicotinic acetylcholine receptor CHRNA3/5 genes and has also

61 been associated with increased nicotine dependence and smoking behavior, and lung
62 cancer (Amos et al., 2008; Carlier et al., 2021; Cui et al., 2014; Hobbs et al., 2017; Hung
63 et al., 2008; Pillai et al., 2009; Wilk et al., 2012). Recent work has demonstrated a role for
64 CHRNA5 in the formation of COPD-like lesions in the respiratory epithelium
65 independently of cigarette smoke, suggesting a direct involvement of nAchRs in shaping
66 epithelial integrity (Routhier et al., 2021). The endogenous ligand of nAchR, acetylcholine
67 (Ach), is a classic neurotransmitter synthesized by Choline Acetyltransferase (ChAT) in
68 cholinergic neurons, as well as in immune cells and epithelial cells, such as brush/tuft
69 cells (Kummer & Krasteva-Christ, 2014; Wessler & Kirkpatrick, 2008). Such cells
70 orchestrate type 2 inflammatory responses (O'Leary et al., 2019; Sell et al., 2021),
71 mucociliary clearance (Perniss et al., 2020) and limit biliary inflammation (O'Leary et al.,
72 2022; O'Leary et al., 2019). How Ach influences homeostasis of barrier epithelia and how
73 disease-associated nAchR variants perturb epithelial function remains mostly unclear.

74 Overall, experimental evidence for the involvement of specific genes associated with the
75 COPD risk loci identified in these studies is mostly lacking, and will be essential for the
76 development of therapeutic strategies targeting novel pathways. Here, we have used the
77 *Drosophila* midgut as a genetically accessible model for epithelial barrier homeostasis to
78 interrogate genes predicted to be involved in COPD based on GWAS studies. The
79 *Drosophila* intestine is lined by a pseudostratified epithelium consisting of enterocytes
80 (ECs) and enteroendocrine cells (EEs) that are regenerated from a basal population of
81 intestinal stem cells (ISCs) (Miguel-Aliaga et al., 2018). In its structure, cell composition
82 and molecular regulation of regenerative processes, the fly intestinal epithelium
83 resembles mammalian airway epithelia (Biteau et al., 2011).

84 Under stress conditions, in response to enteropathogen infection, as well as during
85 normal aging, the fly intestinal epithelium loses its barrier function and exhibits stem cell
86 hyperplasia and commensal dysbiosis (Jasper, 2020). These phenotypes recapitulate
87 changes observed in airway epithelia of COPD patients and can thus be used as a model
88 for pathophysiological changes occurring in this disease (Carlier et al., 2021; Raftery et
89 al., 2020).

90 To assess the role of candidate genes associated with risk alleles in COPD GWAS studies
91 in the maintenance of barrier epithelia integrity, we performed an RNA interference screen
92 perturbing their *Drosophila* orthologues systemically and quantifying the impact of these
93 perturbations on intestinal barrier function. Several of the candidate genes identified in
94 this screen as required for barrier integrity encode for subunits of the nicotinic
95 acetylcholine receptor (nAchR).

96 In the fly intestine, we find that ChAT is expressed by a subset of enteroendocrine cells
97 and that enterocyte-specific expression of nAchR is required for barrier integrity by
98 stimulating chitin release and ensuring maintenance of the peritrophic matrix, a chitinous
99 structure protecting the epithelium from luminal insults. In ECs, Ach is required for the
100 expression of Syt4, a critical regulator of exocytosis (Yoshihara et al., 2005; Zhang et al.,
101 2011) which is required for the maintenance of PM structure and epithelial barrier
102 function. Our data illustrate the usefulness of *Drosophila* as a model for prioritization of
103 potential disease genes identified in GWAS studies, and identify nAchR signaling as a
104 critical mediator of epithelial homeostasis in barrier epithelia.

105

106 **Results**

107 **A genetic screen assessing the role of COPD candidate genes in barrier function**

108 To obtain a curated candidate gene list for COPD, we assigned candidate genes to COPD
109 risk loci (Hobbs et al., 2017) using a combination of expression quantitative trait loci,
110 coding annotation and distance-based metrics (see Methods, Table S1A). *Drosophila*
111 orthologs were identified with the DRSC integrative ortholog prediction tool (DIOPT (Hu
112 et al., 2011)) and corresponding hits with the highest DIOPT score were selected,
113 resulting in a total of 33 *Drosophila* genes screened initially (Fig. 1A).

114 We perturbed these genes systemically by RNA interference (RNAi) in an inducible
115 fashion using the ubiquitous RU486-inducible Gal4 driver Da::GeneSwitch (Da::GS) and
116 scored epithelial barrier dysfunction in homeostatic and stress conditions using the “smurf
117 assay” (Rera et al., 2011). In this approach flies are fed food containing a non-absorbable
118 blue food dye. If the intestinal epithelial barrier is compromised, the dye leaks into the
119 open circulatory system and gives the fly a blue appearance reminiscent of the popular

120 blue cartoon characters. Where available, a minimum of 2 different RNAi lines per gene
121 were included (Table S1B). Female flies carrying the driver and RNAi construct were
122 allowed to mature and mate for 10-12 days before being placed on blue food with RU-
123 486 to induce knockdown for 24h. Since COPD is strongly associated with environmental
124 stress, we then challenged flies with paraquat (N, N'-dimethyl-4,4'-bipyridinium
125 dichloride), a herbicide known to inflict oxidative stress and damage to the fly gut
126 comparable to the effects of cigarette smoke on the lung epithelium (Biteau et al., 2008;
127 Caliri et al., 2021). After 16h paraquat challenge the flies were moved back to blue food
128 containing RU486 and smurf numbers were recorded over the span of about a week (Fig
129 1B). We generated a “barrier dysfunction index” for every RNAi line by calculating the
130 natural logarithm (ln) of the ratio of peak smurf percentage between RNAi line and control
131 knockdown and plotted individual RNAi lines accordingly. A positive index implies an
132 enhancement of barrier dysfunction after depletion, while a negative index suggests
133 rescue of barrier integrity after depletion (Fig. 1C). Based on the outcomes of individual
134 RNAi knockdowns, we assigned an overall rating for each candidate gene (Table S1B).
135 We found that disruption of 18 genes (~55%) resulted in enhancement (e.g. these genes
136 were necessary for barrier integrity), while disruption of 4 genes (12%) resulted in
137 suppression of the barrier dysfunction. The remaining 11 genes did not display any effect
138 on barrier function (Fig. 1D). Out of the 16 of *Drosophila* hits where eqtl data was available
139 for the corresponding human gene, 9 were consistent with the direction of the effect
140 inferred from the association of the COPD risk allele with gene expression (56%, Fig. 1A,
141 Table S1B).

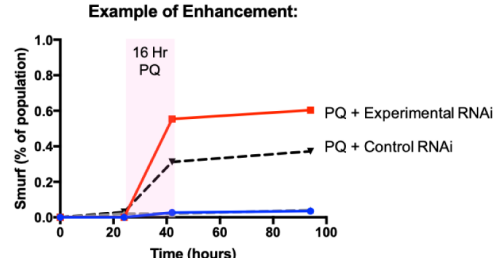
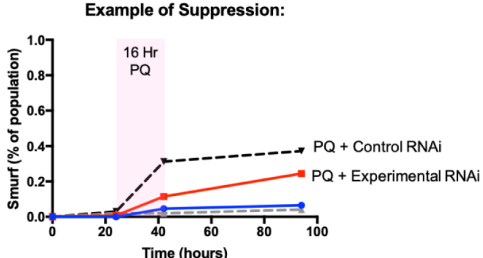
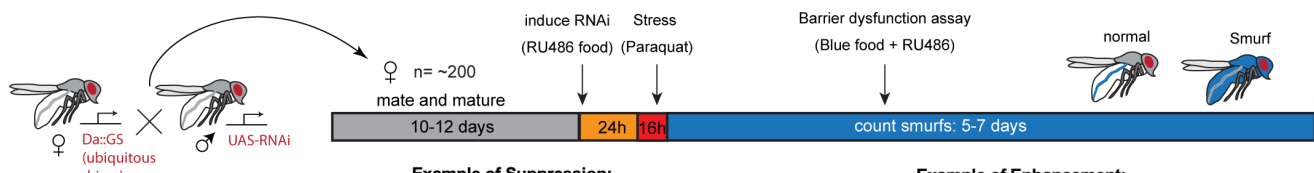
Katheder et al., Fig. 1

A

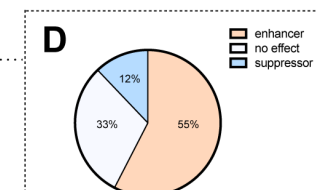
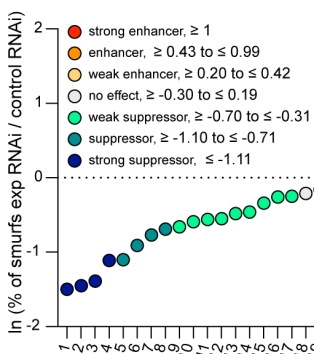
COPD GWAS hits and *Drosophila* candidate orthologues

SNP	CHR	BP	gene	evidence	Drosophila ortholog	Drosophila rating	eqtl direction risk allele	agreement
rs10429950	1	218624533	TGFB2	nearest	myo, daw	enhancer (myo)	not available	N/A
rs6837671	4	89873092	FAM13A	nearest	CG6424	suppressor	not available	N/A
rs2806356	6	109266255	ARMC2	nearest	CG32668	no effect	not available	N/A
rs754388	14	93115410	RIN3	coding,eqtl	spri	no effect	higher expression	N/A
rs1441358	15	71612514	THSD4	eqtl	loh	no effect	higher expression	N/A
rs12459249	19	41339896	CYP2A6	nearest	Cyp18a1, Cyp305a1	enhancer	not available	N/A
rs2955083	3	127961178	EEFSEC	eqtl	eEFSec	suppressor	higher expression	Yes
rs2955083	3	127961178	RUVBL1	eqtl	pont	no effect	lower expression	N/A
rs11727735	4	106631870	GSTCD	eqtl	CG10428	enhancer	lower expression	Yes
rs11727735	4	106631870	INTS12	eqtl	Ints12	no effect	higher expression	N/A
rs113897301	5	156929077	ADAM19	eqtl	Meltrin	enhancer	higher expression	No
rs113897301	5	156929077	NIPAL4	eqtl	spict	no effect	higher expression	N/A
rs2076295	6	7563232	DSP	eqtl	shot	suppressor	higher expression	Yes
rs721917	10	81706324	SFTP2D	coding,eqtl	lectin-28C	no effect	higher expression	N/A
rs17486278	15	78867482	CHRNA3	eqtl	nAChR β 2, nAChR α 4	enhancer	lower expression	Yes
rs17486278	15	78867482	CHRNA5	coding,eqtl	nAChR α 1, nAChR α 2, nAChR α 3	enhancer	inconsistent	N/A
rs17486278	15	78867482	PSMA4	eqtl	Prosa3	no effect	higher expression	N/A
rs17707300	16	28593347	APOBR	coding	Muc11a	enhancer	not available	N/A
rs17707300	16	28593347	EIF3C	eqtl	elf3c	enhancer	higher expression	No
rs17707300	16	28593347	EIF3CL	eqtl	elf3c	enhancer	higher expression	No
rs17707300	16	28593347	NFATC2IP	eqtl	Rad60	enhancer	higher expression	No
rs17707300	16	28593347	NUPR1	eqtl	CG6770	enhancer	lower expression	Yes
rs17707300	16	28593347	SH2B1	eqtl	Lnk	enhancer	lower expression	Yes
rs17707300	16	28593347	SPNS1	eqtl	spin	suppressor	higher expression	Yes
rs17707300	16	28593347	SULT1A1	coding,eqtl	St1	enhancer	lower expression	Yes
rs17707300	16	28593347	SULT1A2	coding,eqtl	St1	enhancer	higher expression	No
rs17707300	16	28593347	TUFM	eqtl	mEFTu1	enhancer	higher expression	No
rs7186831	16	75473155	BCAR1	eqtl	p130CAS	no effect	inconsistent	N/A
rs7186831	16	75473155	CFDP1	eqtl	Yeti	no effect	lower expression	N/A
rs7186831	16	75473155	TMEM170A	eqtl	CG12341	enhancer	higher expression	No

B



C



143 **Figure 1: A *Drosophila* screen for COPD-associated candidate genes**

144 A) List of human candidate genes for genetic loci associated with COPD risk and their *Drosophila*
145 orthologs. An overall rating was assigned to the *Drosophila* genes based on the detailed results
146 of the individual RNAi lines included in the screen: Genes exacerbating barrier dysfunction upon
147 depletion were categorized as enhancers, while genes whose depletion improved barrier function
148 were rated as suppressors of barrier dysfunction (Table S1B). When available, the human risk
149 allele expression data is compared to the results of the *Drosophila* screen (agreement column).
150 (SNP, Single nucleotide polymorphism; CHR, chromosome; BP, base pair number; eqtl,
151 expression quantitative trait loci).
152 B) Experimental design of intestinal barrier function screen. Flies carrying the ubiquitous driver
153 Da::GS were crossed to RNAi lines targeting candidate genes. The female offspring was aged for
154 10-12 days before induction of RNAi expression by RU-486 for 24h on blue food. Flies were
155 challenged with sucrose alone (mock) or 25mM Paraquat for 16h overnight and then placed back
156 on blue food. Blue flies with a defective intestinal barrier("smurfs") were counted daily for 5-7 days.
157 C) Ranking of screened RNAi lines based on the natural logarithm (ln) of the ratio between the
158 proportion of smurfs after candidate gene knockdown and luciferase RNAi control. Each number
159 corresponds to an RNAi line listed in Table S1B. Cut offs for the different categories are indicated.
160 D) Summary of screen results based on broad categorization as enhancer, suppressor or no
161 effect. If several RNAi lines targeting the same gene unanimously had no effect, the gene was
162 rated "no effect, conclusive", while inconsistent results were rated "no effect, inconclusive". For
163 details see Table S1B.

164

165

166 **nAchR subunit expression in ECs is required for barrier function**

167 Our initial screen identified disruption of 5 nAchR subunits as a strong enhancers of
168 barrier dysfunction. Ubiquitous knockdown of various nAchR subunits with Da::GS lead
169 to mild barrier dysfunction under homeostatic conditions, and greatly enhanced barrier
170 dysfunction after paraquat challenge (Fig. 2A, Fig. S1A), suggesting a sensitization of the
171 epithelium to stress.

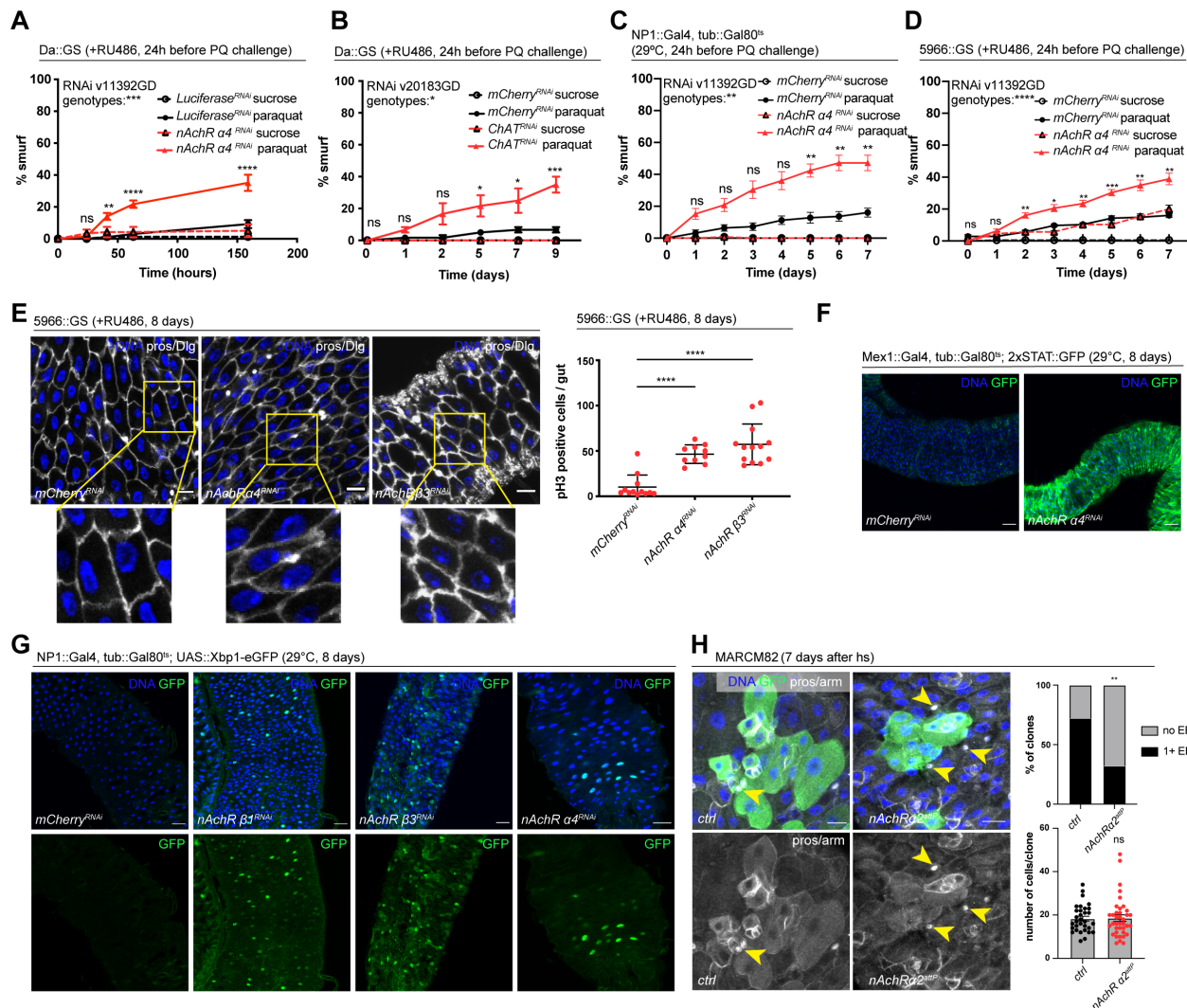
172 Acetylcholine (Ach) is the physiological ligand for nAchRs and is produced by ChAT, an
173 enzyme that catalyzes the transfer of an acetyl group from coenzyme acetyl-CoA to
174 choline (Taylor P., 1999). Modulation of total organismal Ach levels by RNAi-mediated
175 silencing of ChAT under control of Da::GS also resulted in increased barrier dysfunction
176 after paraquat exposure (Fig. 2B, Fig. S1B), further supporting the role of Ach/nAChR
177 signaling in maintaining intestinal epithelial homeostasis.

178 To investigate a possible direct intestinal role for nAchR, and to identify the requirement
179 for individual subunits, we used the drivers 5966::GS and NP1::Gal4 to separately deplete
180 nAchR subunits. These drivers induce expression of UAS-linked transgenes in
181 enteroblasts and enterocytes (Jiang et al., 2009; Zeng & Hou, 2015). While 5966::GS is
182 inducible using RU486, we combined NP1::Gal4 with tub::G80ts (NP1ts) to allow for
183 temperature-mediated induction (TARGET system (McGuire et al., 2004)) before
184 subjecting the flies to paraquat. Knockdown of nAchR α 4 or β 3 with both drivers increased
185 the numbers of smurf flies, indicating a defective epithelial barrier (Fig. 2C, D, Fig. S1C,
186 D).

187 Knockdown of nAchR in ECs resulted in various hallmarks of epithelial stress. These
188 include a mildly disorganized epithelial morphology (visualized by staining for the septate
189 junction marker Dlg) and induction of intestinal stem cell (ISC) proliferation (Fig. 2E),
190 presumably due to stress signals released by ECs (Biteau et al., 2011), as well as
191 activation of JAK/STAT signaling (measured using the 10xSTAT::GFP reporter (Bach et
192 al., 2007)) and ER stress signaling (measured using an Xbp1::GFP reporter (Sone et al.,
193 2013) (Fig. 2F, G). Interestingly, Dlg staining did not indicate a strong disruption of EC
194 junctions in the epithelium, suggesting that barrier dysfunction may be caused by a
195 separate mechanism.

196 To further confirm and characterize the role for nAchR subunits in epithelial homeostasis,
197 we generated MARCM mutant clones (Lee & Luo, 2001) lacking *nAChRa2* using the null
198 allele *nAChRa2*^{attP} generated by CRISPR/Cas9 based homologous recombination
199 resulting in the introduction of an attP site, 3xP3-RFP and a loxP site (Deng et al., 2019;
200 Lu et al., 2022). Clone formation, growth, and cell composition also provide insight into a
201 possible role of *nAChRa2* in ISC proliferation and differentiation. While *nAChRa2*^{attP}
202 clones grew to similar cell numbers as their control counterparts, they failed to produce
203 normal numbers of EEs, as only 32% of *nAChRa2* clones contained at least 1 EE
204 compared to 72% of clones in the control samples (Fig. 2H). In addition to a broader role
205 for nAchR in maintaining barrier integrity, nAchR may thus also be required for the proper
206 differentiation of EEs. Whether this effect on EE differentiation contributes to the barrier
207 dysfunction remains unclear.

Katheder et al., Fig. 2



208

209 **Figure 2: nAchR genes are required for barrier function in enterocytes (ECs) and**
 210 **enteroendocrine (EEs) cell differentiation**

211 A) Barrier dysfunction assay after Luciferase (control) or nAchR α4 subunit depletion for 24h with
 212 ubiquitous driver Da::GS. nAchR α4: n=100 for Luciferase RNAi (control) on sucrose; n=125
 213 animals for Luciferase RNAi on sucrose+paraquat; n=150 for nAchR α4 RNAi on sucrose; n=175
 214 animals for nAchR α4 on sucrose+paraquat. Paraquat concentration 25mM. N=1. Two-way
 215 ANOVA followed by Šídák's multiple comparisons test.

216 B) Barrier dysfunction assay after mCherry (control) or ChAT depletion for 24h with ubiquitous
 217 driver Da::GS. n=75 animals per genotype and condition; N=3. Two-way ANOVA followed by
 218 Šídák's multiple comparisons test.

219 C) Barrier dysfunction assay after mCherry (control) or nAchR α4 depletion for 24h with
 220 enterocyte-specific driver NP1::Gal4, tub::Gal80^{ts} (NP1^{ts}). n=125 animals per genotype and
 221 condition; N=3. Two-way ANOVA followed by Šídák's multiple comparisons test.

222 D) Barrier dysfunction assay after mCherry (control) or nAchR $\alpha 4$ depletion for 24h with
223 enterocyte-specific driver 5966::GS. n=175 animals per genotype and condition; N=3. Two-way
224 ANOVA followed by Šídák's multiple comparisons test.

225 E) Confocal immunofluorescence images examining epithelial organization and quantification of
226 ISC mitoses in guts depleted of nAchR $\beta 3$ and $\alpha 4$ subunits in ECs for 8 days. Septate junctions
227 are stained with anti-Dlg antibody (white), DNA (blue) is labeled with Hoechst. Yellow boxed insets
228 are shown enlarged in bottom row. Scale bars 10 μ m.

229 Mitotically active ISCs are labeled with anti-pH3 antibody; n=12;10;13 guts for mCherry (control),
230 nAchR $\alpha 4$ and nAchR $\beta 1$, respectively. N=3. Ordinary one-way ANOVA followed by Dunnett's
231 multiple comparisons test.

232 F) Confocal microscopy images of guts expressing a 2xSTAT::GFP reporter (green) depleted of
233 mCherry (control) or nAchR $\alpha 4$ for 8 days in ECs with Mex::Gal4, tub::Gal80^{ts}. n=10 guts per
234 genotype. N=3. Scale bar 50 μ m.

235 G) Confocal immunofluorescence image of posterior midguts expressing the UPR-reporter UAS-
236 Xbp1-EGFP (green) after 8 days of nAchR subunit knockdown by RNAi. The EGFP tag is only in
237 frame with the Xbp1(s) coding sequence after splicing using the unconventional splice site, which
238 occurs under stress conditions. DNA (blue) is labeled with Hoechst. n=8 guts per genotype. N=3.
239 Scale bar 25 μ m.

240 H) Confocal immunofluorescence images of wildtype and nAchR $\alpha 2$ MARCM clones (green) 7
241 days after heat shock. Stem cells and enteroblasts are stained with anti-armadillo antibody
242 (white); EEs are labeled with anti-prospero antibody (white, nuclear signal highlighted with yellow
243 arrowheads) and DNA (blue) is labeled with Hoechst. Scale bars 15 μ m. Quantification of EE
244 numbers within clones: n=32;38 clones for wildtype or nAchR $\alpha 2$, respectively from 3 pooled
245 experiments. Fisher's exact test. Quantification of cell numbers/clone: n=32;38 clones for wildtype
246 or nAchR $\alpha 2$, respectively from 3 pooled experiments. Unpaired two-tailed t-test.

247

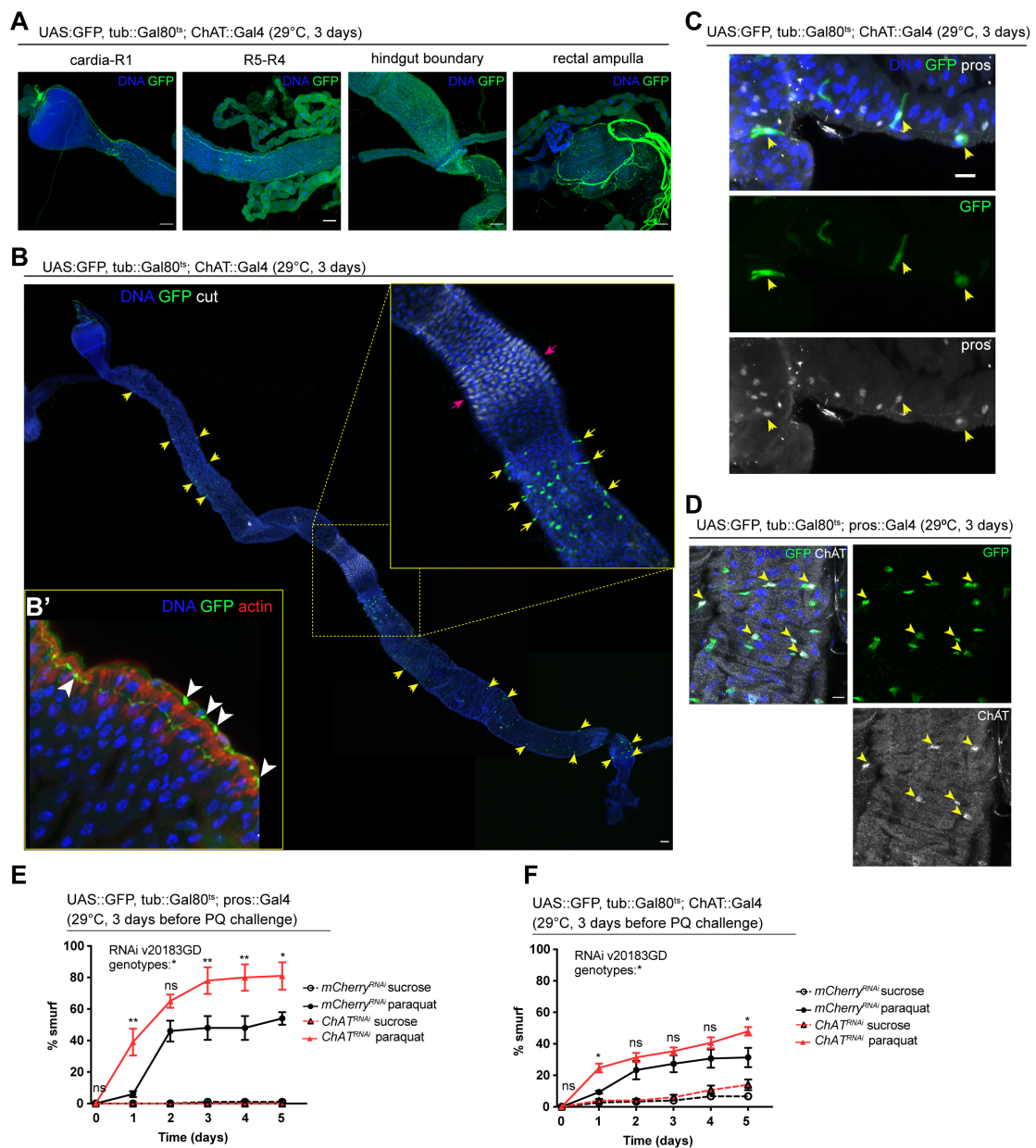
248

249 **Acetylcholine promotes barrier function**

250 We sought to identify the source of Ach activating these receptors in the gut epithelium
251 next. Because of its well understood role as a neurotransmitter, we initially focused on
252 the innervation of the fly gut, which has been described previously (Cognigni et al., 2011).
253 Expression of UAS::GFP under the control of ChAT::Gal4 confirmed that some of these
254 neurons are indeed cholinergic (Fig. 3A, B'). Upon closer examination of the epithelium,
255 we also noticed a small subset of prospero-positive EEs expressing GFP, predominantly
256 located in the R4 and R5 regions of the midgut (Fig. 3B, C). In addition, labeling of guts
257 expressing GFP under the control of neuron and EE-driver, prospero-Gal4, combined
258 with tub::Gal80^{ts} (pros^{ts}) with a ChAT antibody confirmed ChAT expression in a subset of
259 EEs (Fig. 3D).

260 To address the role of Ach production in barrier integrity, we depleted ChAT with *pros*^{ts},
 261 as well as with ChAT::Gal4. Reduction of ChAT levels with both drivers rendered flies
 262 more susceptible to barrier dysfunction after paraquat exposure (Fig. 3E, F).
 263 Combined, these data support the notion that Ach signaling is critical to maintain barrier
 264 integrity and stress resilience in the intestinal epithelium of the fly. While cholinergic
 265 innervation is a likely source of the ligand in this response, local production of Ach by
 266 enteroendocrine cells may also play a role in maintaining homeostasis.

Katheder et al., Fig. 3



267

268 **Figure 3: Acetylcholine produced in EEs and/or neurons promotes barrier function**

269 A) Confocal immunofluorescence image of cholinergic innervation of different intestinal
270 compartments. GFP (green) expression is driven by Mi{Trojan-GAL4.0}ChAT[MI04508-TG4.0]
271 CG7715[MI04508-TG4.0-X] and detected in the anterior (cardia/R1) as well as posterior midgut
272 (R4-R5), at the hindgut boundary and rectal ampulla. DNA (blue) is labeled with Hoechst. n=5
273 guts. N=3. Scale bars 50 μ m.
274 B) Stitched confocal immunofluorescence images of a gut expressing GFP (green) under control
275 of Mi{Trojan-GAL4.0}ChAT[MI04508-TG4.0] CG7715[MI04508-TG4.0-X], stained with anti-cut
276 antibody (white). Yellow arrows indicate GFP-positive cells. Enlarged insert shows GFP-positive
277 cells adjacent to the gastric region labeled with cut (pink arrows). DNA (blue) is labeled with
278 Hoechst. n=5 guts. N=3. Scale bar 50 μ m.
279 B') Confocal image of a gut expressing GFP (green) under control of Mi{Trojan-
280 GAL4.0}ChAT[MI04508-TG4.0] CG7715[MI04508-TG4.0-X], stained with Phalloidin (red).
281 Transverse section of the epithelium is shown revealing inter-epithelial axons from ChAT+
282 neurons. White arrowheads highlight axonal boutons. n=5 guts. N=3
283 C) Fluorescent immunohistochemistry image of posterior midgut expressing GFP (green) under
284 the control of Mi{Trojan-GAL4.0}ChAT[MI04508-TG4.0] CG7715[MI04508-TG4.0-X], stained with
285 anti-prospero antibody (white). Arrows indicate GFP-positive cells that also label for pros. DNA
286 (blue) is labeled with Hoechst. n=8 guts. N=3. Scale bar 10 μ m.
287 D) Confocal immunofluorescence image of ChAT antibody staining of the posterior midgut. EEs
288 are expressing GFP (green) driven by pros::Gal4, yellow arrows indicate the overlap between
289 ChAT staining (white) and pros-positive cells. DNA (blue) is labeled with Hoechst. n=8 guts. N=3.
290 Scale bar 10 μ m.
291 E) Barrier dysfunction assay after mCherry (control) or ChAT knockdown in EEs for 3 days with
292 prospero-Gal4. n=100 animals per genotype and condition; N=3. Two-way ANOVA followed by
293 Šídák's multiple comparisons test.
294 F) Barrier dysfunction assay after mCherry (control) or ChAT knockdown with Mi{Trojan-
295 GAL4.0}ChAT[MI04508-TG4.0] CG7715[MI04508-TG4.0-X] for 3 days. n=120 animals per
296 genotype and condition; N=3. Two-way ANOVA followed by Šídák's multiple comparisons test.
297 Data presented as mean \pm SEM. ns, not significant, P > 0.05; *P \leq 0.05; **P \leq 0.01; ***P \leq 0.001;
298 ****P \leq 0.0001. n: number of animals or midguts analyzed; N: number of independent experiments
299 performed with similar results and a similar n
300

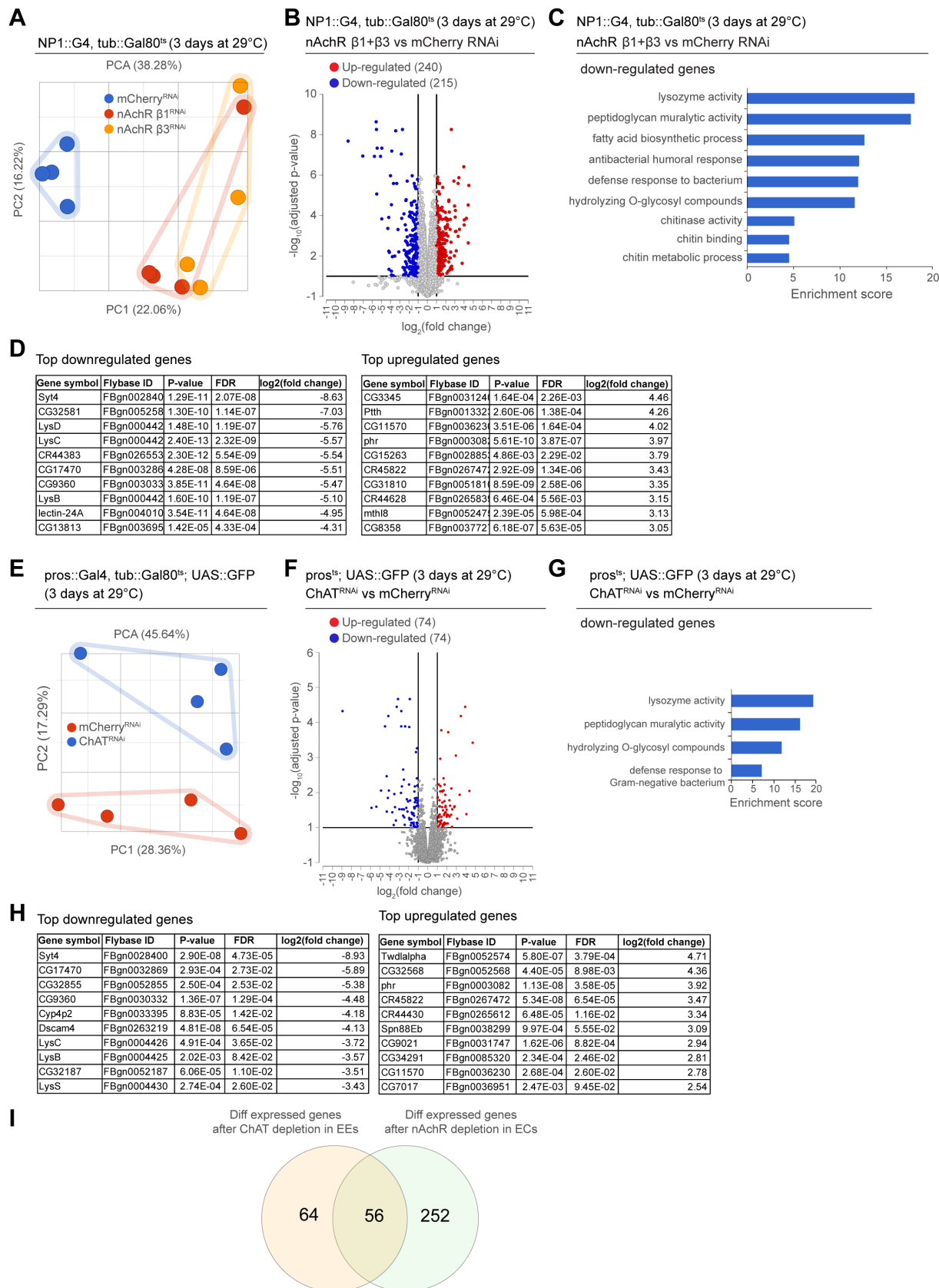
301 **Transcriptional changes after disruption of Ach signaling in the intestinal
302 epithelium**

303 As we observed barrier dysfunction without obvious deregulation of epithelial junctions
304 after nAChR loss in ECs, we decided to profile changes in gene expression elicited in the
305 gut by nAChR depletion. We performed RNAseq on whole guts depleted for nAChR β 1 or
306 β 3 for 3 days under the control of NP1^{ts}. PCA analysis suggested that the transcriptomes
307 from intestines with nAChR knockdown were clearly distinct from transcriptomes of
308 intestines with a control RNAi construct (mCherry RNAi; Fig. 4A). Overall, we observed

309 240 upregulated and 215 downregulated genes (Fig. 4B; FDR \leq 0.1; log₂(fold change)
310 < -1 or > 1; 100% of samples have \geq 1 reads), of which 171 were differentially expressed
311 in both nAChR β 1 and β knockdowns, supporting the idea that these subunits have
312 partially overlapping functions (Fig. 4B, Fig. S2A, E). Synaptotagmin 4 (Syt4) was the
313 most significantly downregulated gene in both knockdowns (Fig. 4D). GO term
314 enrichment analysis revealed increased expression of glucosidases and hydrolases after
315 nAChR knockdown (Fig. S2B, E), and downregulation of genes involved in immune
316 responses such as lysozymes (Fig. 4C, Fig. S2C) and genes related to chitin binding and
317 metabolism.

318 In parallel, we analyzed the transcriptome of whole guts depleted of ChAT using pros^{ts}
319 for 3 days. While the knockdown samples also separated clearly from the control, they
320 displayed fewer differentially regulated genes than guts depleted of nAChR (Fig. 4E, F,
321 Fig. S2F). However, Syt4 remained the most significantly downregulated gene (Fig. 4H)
322 and enriched GO terms overlapped significantly with the previous experiment, especially
323 with regards to immune responses as well as chitin metabolism (Fig. 4G, Fig. S2D). Direct
324 comparison of differentially regulated genes revealed an overlap of 56 genes between
325 guts depleted for nAChR in ECs and guts where ChAT was silenced using pros^{ts} (Fig. 4I).

Katheder et al., Fig. 4



327 **Figure 4: Transcriptional changes after disruption of Ach signaling in the intestinal**
328 **epithelium**

329 A) PCA plot of samples after 3 days of nAchR subunit depletion by RNAi in enterocytes with NP1^{ts}.
330 n=4 samples. N=1.

331 B) Volcano plot showing significantly differentially regulated genes after short-term nAchR $\beta 1$ or
332 $\beta 3$ knockdown in enterocytes. (FDR ≤ 0.1 ; log₂(fold change) < -1 or > 1 ; 100% of samples have
333 ≥ 1 reads)

334 C) Gene set enrichment analysis of significantly downregulated genes after nAchR $\beta 1$ and $\beta 3$
335 knockdown in ECs.

336 D) Top 10 most down- or upregulated genes after 3 days of nAchR subunit depletion by RNAi in
337 enterocytes with NP1^{ts}.

338 E) PCA analysis after 3 days of ChAT depletion with RNAi in EEs under control of pros^{ts}. n=4
339 samples. N=1.

340 F) Volcano plot of significantly differentially regulated genes after 3 days of ChAT knockdown in
341 EEs. (FDR ≤ 0.1 ; log₂(fold change) < -1 or > 1 ; 100% of samples have ≥ 1 reads)

342 G) Gene set enrichment analysis of significantly downregulated genes after ChAT depletion in
343 EEs.

344 H) Top 10 most down- or upregulated genes after 3 days of ChAT knockdown by RNAi in EEs
345 with pros^{ts}.

346 I) overlap between differentially regulated genes after 3 days knockdown of ChAT in EEs or
347 nAchR $\beta 1$ and $\beta 3$ in ECs.

348 n: number of samples included; N: number of independent experiments performed with similar
349 results and a similar n.

350

351 **nAchR depletion disrupts PM integrity**

352 The enrichment of chitin GO terms in our RNAseq experiments prompted us to examine
353 the peritrophic matrix (PM). The PM is a protective structure lining the gut of many insects,
354 consisting of crosslinked glycoproteins, proteoglycans and chitin (Erlandson et al., 2019;
355 Hegedus et al., 2009; Hegedus et al., 2019). It surrounds the food bolus and forms a
356 selectively permeable physical barrier preventing direct contact between abrasive food
357 particles and bacteria with the epithelium, thus helping to compartmentalize digestive
358 processes as well as protecting the animal from ingested toxins and pathogens
359 (Erlandson et al., 2019; Hegedus et al., 2019). In flies, it was shown that the PM protects
360 against pathogenic bacteria and their pore-forming toxins, such as *Pseudomonas*
361 *entomophilia* and *Serratia marcescens* (Kuraishi et al., 2011). Dipteran insects such as
362 *Drosophila* are thought to continuously produce a type II PM originating in the cardia at
363 the anterior end of the midgut (Hegedus et al., 2019). There is evidence suggesting

364 remodeling activity along the posterior midgut, as transcripts for PM components were
365 found enriched in the R4 region of the midgut (Buchon et al., 2013). Moreover, intestinal
366 IMD signaling as well as a subset of enteric neurons have been implicated in modulating
367 the composition and permeability of the PM, however the underlying molecular
368 mechanisms of PM remodeling remain poorly understood (Buchon, Broderick, Poidevin,
369 et al., 2009; Kenmoku et al., 2016).

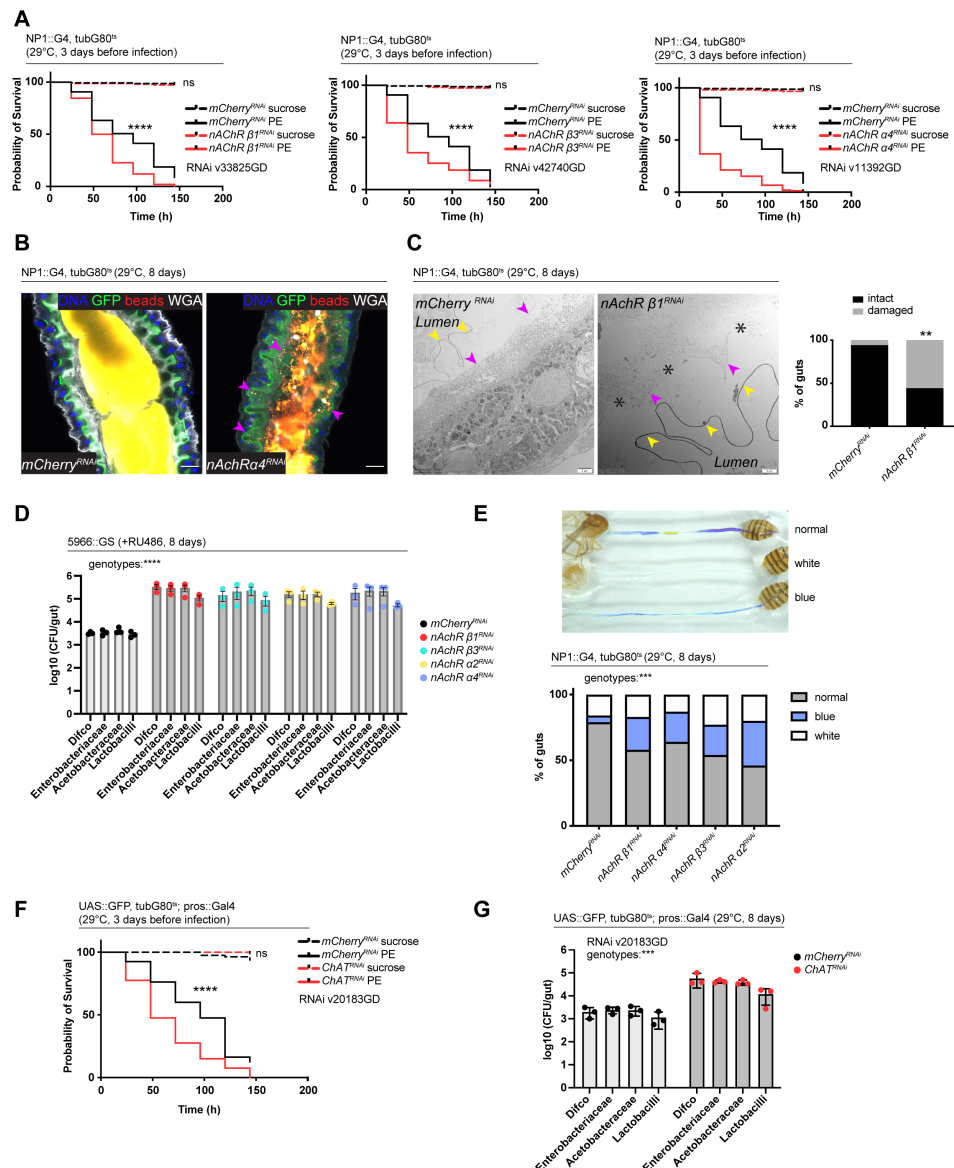
370 Transcript levels of two components of the PM, Crys and CG32302, were noticeably
371 reduced in guts depleted of nAchR subunits (Fig. S3A). Earlier studies highlighted the
372 importance of the PM in protecting the animal against lethal pathogenic bacterial infection
373 with *Pseudomonas entomophila* (PE) (Kuraishi et al., 2011). Indeed, depletion of nAchR
374 subunits in ECs significantly reduced survival after PE infection (Fig. 5A).

375 Defects in the PM can be visualized with confocal light microscopy by feeding animals
376 fluorescently labeled latex beads that are retained in the food bolus and stay separated
377 from the epithelium if the PM sleeve is intact (Kenmoku et al., 2016). The surface of the
378 bead-containing ingested food appeared relatively smooth in control animals. In contrast,
379 silencing of nAchR $\beta 1$ or $\beta 3$ led to spiny protrusions of the fluorescent matter, indicating
380 a damaged PM (Fig. S3B). We further modified this assay by crossing in the brush border
381 marker A142::GFP (Buchon et al., 2013) and visualizing the PM with fluorescently labeled
382 wheat germ agglutinin (WGA), a lectin that recognizes chitin (Carlini & Grossi-de-Sá,
383 2002), in addition to feeding the latex beads. Guts depleted of nAchR $\alpha 4$ displayed
384 fluorescent signal scattered throughout the lumen and making contact with the brush
385 border while the beads stayed confined to the PM sleeve and separated from the
386 epithelium in control guts (Fig. 5B).

387 Electron microscopy has been successfully applied to detect subtle defects in PM
388 morphology (Kuraishi et al., 2011). We therefore performed an ultrastructural analysis of
389 the R4 compartment of guts depleted of nAchR $\beta 1$. The PM was visible as a continuous
390 folded ring in the lumen of control flies, consisting of electron-dense membranous material
391 of roughly 100-200 nm thickness. Additionally, a second, much thinner (15-20nm)
392 membranous ring-shaped layer was observed between the PM and the apical surface of
393 the epithelial cells (Fig. 5C, Fig. S3C).

394 In the majority of the 18 examined nAChR β 1 knockdown midguts the thick PM layer was
 395 not compromised (Fig. S3D). However, in 56% of samples the thin layer was clearly
 396 disrupted or missing altogether (Fig. 5C). Notably, none of the guts presented an intact
 397 thin layer in the absence of the thick layer. In all examined control and knockdown guts,
 398 the septate junctions connecting adjacent cells appeared normal, consistent with our Dlg
 399 staining, as well as the fact that no changes in junctional protein expression was observed
 400 in our RNAseq experiments.

Katheder et al., Fig. 5



401

402 **Figure 5: nAchR depletion disturbs PM integrity, causes dysbiosis and**
403 **inflammation**

404 A) Survival of animals depleted for mCherry (control) or nAchR $\beta 1$, $\beta 3$ or $\alpha 4$ for 3 days before
405 *Pseudomonas entomophila* infection. n=150 animals per genotype and condition; N=3. Log Rank
406 (Mantel-Cox) test.

407 B) Confocal immunofluorescence image of posterior midguts depleted for either mCherry (control)
408 or nAchR $\alpha 4$ for 8 days. Animals are expressing a GFP-brush border marker (green) and were
409 fed red fluorescent beads to assess peritrophic matrix (PM) integrity (beads appear yellow/orange
410 due to autofluorescence of beads in GFP channel). PM is labeled with WGA (white), DNA (blue)
411 is labeled with Hoechst. Pink arrowheads highlight beads no longer contained by the PM sleeve.
412 n=15 guts per genotype. N=3. Scale bar 20 μ m.

413 C) Electron microscopy images and quantification of thin PM layer integrity. Thick (yellow arrows)
414 and thin (pink arrows) PM layers are indicated. Asterisks highlight gaps in the thin layer after
415 nAchR $\beta 1$ depletion. n=16; 18 midguts. N=1. Fisher's exact test.

416 D) Colony forming units (CFU) of whole guts plated on selective growth media after 8 days of
417 nAchR subunit depletion in ECs. 3 pooled independent experiments are shown. n=5 pooled
418 animals per genotype and experiment. Two-way ANOVA.

419 E) Gut compartmentalization and acidity after mCherry (control) or nAchR $\beta 1$, $\beta 3$ or $\alpha 4$ depletion
420 for 8 days. Healthy flies fed with Bromphenol blue pH indicator display an acidic patch (yellow),
421 while loss of gut compartmentalization leads to all blue or white guts. n=87 guts for mCherry
422 (control), n=93 guts for nAchR $\beta 1$, n=113 guts for nAchR $\alpha 4$, n=87 guts for nAchR $\beta 3$ and n=90
423 guts for nAchR $\alpha 2$. 4 independent pooled experiments are shown. Chi square test.

424 F) Survival after 3 days of mCherry (ctrl) or ChAT depletion in EEs followed by *Pseudomonas*
425 *entomophila* infection. n=80 animals per genotype and condition; N=3. Log Rank (Mantel-Cox)
426 test.

427 G) Colony forming units (CFU) of whole guts plated on selective growth media after 8 days of
428 ChAT depletion in EEs. 3 pooled independent experiments are shown. n=5 pooled animals per
429 genotype and experiment. Two-way ANOVA.

430 Data presented as mean \pm SEM. ns, not significant, P > 0.05; *P \leq 0.05; **P \leq 0.01; ***P \leq 0.001;
431 ****P \leq 0.0001. n: number of animals or midguts analyzed; N: number of independent experiments
432 performed with similar results and a similar n.

433

434 **Defects in Ach signaling disturb gut compartmentalization and cause dysbiosis**
435 **and JAK-STAT-mediated inflammation**

436 Since the PM has been connected to regulation of the microbiome in mosquitos (Rodgers
437 et al., 2017), we hypothesized that nAchR silencing also deregulates the microbial
438 community inhabiting the fly gut. To test this assumption, we measured microbial load by
439 plating pooled guts of control or nAchR knockdown animals on selective media supporting
440 the growth of commensals such as Lactobacilli, Acetobacteriaceae or
441 Enterobacteriaceae. The amount of CFUs after 8 days of nAchR $\beta 1$, $\beta 3$ or $\alpha 4$ silencing

442 exceeded control levels significantly, indicating that these flies struggle to maintain
443 appropriate commensal numbers (Fig. 5D). The fly midgut is functionally
444 compartmentalized and contains a stomach-like region of acid-producing copper cells
445 (Dubreuil, 2004). A previous study has highlighted the importance of gut
446 compartmentalization in controlling microbiome abundance and distribution. As flies age,
447 this spatial organization is progressively lost due to chronic JAK-STAT activation leading
448 to metaplasia of copper cells in the acidic gastric region, ultimately resulting in dysbiosis
449 and death of the animal (Li et al., 2016). Gut compartmentalization can be visualized by
450 feeding flies the pH indicator Bromphenol blue, which labels the acidic copper cell region
451 in yellow, while the rest of gut remains blue, indicative of a more basic pH (Li et al., 2016).
452 Reduction of nAchR levels lead to an increase of disturbed acidity patterns, ranging from
453 completely blue guts to samples with weak staining and white patches, which has been
454 attributed to expansion of acid-producing commensals like *Lactobacillus* along the whole
455 gut (Li et al., 2016) (Fig. 5E).

456 Dysbiosis can be a consequence of IMD pathway disruption, but at the same time
457 triggers chronic IMD pathway activation (Buchon, Broderick, Chakrabarti, et al., 2009;
458 Guo et al., 2014) Surprisingly, we did not observe an upregulation of antimicrobial
459 peptides (AMP) transcripts classically associated with an IMD response (De Gregorio et
460 al., 2002; Imler & Bulet, 2005).

461 Furthermore, depletion of ChAT in EEs with pros^{ts} also caused increased susceptibility to
462 PE infection (Fig. 5F) as well as dysbiosis (Fig. 5G). Conversely, overexpression of ChAT
463 promoted survival after bacterial infection (Fig. S3E).

464 Together these results suggest that Ach signaling is required to maintain a healthy
465 microbiome and protect the animals against pathogenic infections.

466

467 **Syt4 is a transcriptional target of nAchR regulating PM function**

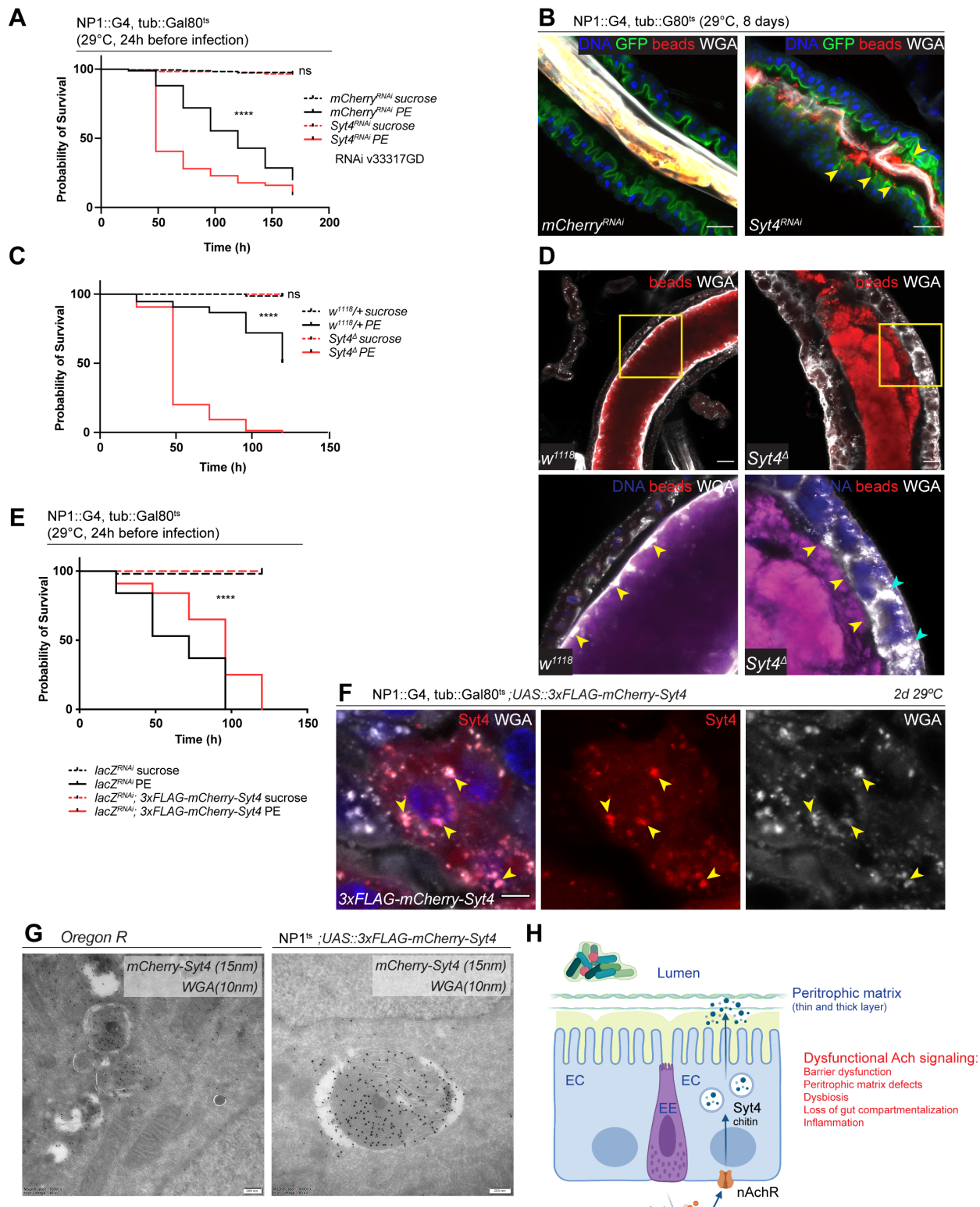
468 One of the most significantly downregulated genes identified in our RNAseq data sets is
469 Synaptotagmin 4, a vesicular Ca²⁺-binding protein promoting retrograde signaling at
470 synapses (Yoshihara et al., 2005). RNAi-mediated silencing of Syt4 under control of

471 NP1^{ts} reduced survival after challenge with PE (Fig. 6A, Fig. S4A) and caused PM defects
472 visualized with the bead feeding assay (Fig. 6B). Moreover, Syt4 depletion increased
473 commensal numbers (Fig. S4B), disrupted gut compartmentalization (Fig. S4C) as well
474 as the morphology of the gastric region: Acid-producing copper cells usually form deep
475 invaginations of the apical membrane (Dubreuil, 2004), giving rise to a gastric unit that
476 can be visualized with anti-cut staining (Li et al., 2016). Syt4-depletion resulted in a
477 disorganized morphology and a marked flattening of these units (Fig. S4D).

478 We generated a new Syt4 null mutant with CRISPR/Cas9 technology to further
479 substantiate these findings. While these mutant animals were homozygous viable, they
480 displayed enhanced susceptibility to PE challenge (Fig. 6C) and a fragmented PM, often
481 accompanied by enlarged WGA-positive structures within the epithelium (Fig. 6D).

482 To characterize the localization of Syt4 in the gut epithelium we utilized a 3xFLAG-
483 mCherry-labeled protein trap line under UAS control (Singari et al., 2014).
484 Overexpression of this construct with NP1^{ts} had a protective effect on animal survival after
485 PE challenge (Fig. 6E) and yielded a vesicular staining pattern that overlapped with Golgi
486 and lysosomal markers (Fig. S4E). Interestingly, we noticed a significant colocalization of
487 Syt4-mCherry-positive structures and WGA staining in immunofluorescence experiments,
488 suggesting that Syt4 vesicles contain chitin (Fig. 6F). Immunogold electron microscopy
489 confirmed the colocalization of Syt4-mCherry and WGA in vesicular structures containing
490 highly folded membrane swirls and amorphous cargo (Fig. 6G). These vesicles also
491 stained positive for the late endosomal/lysosomal marker Lamp1 (Fig. S4F). Similar
492 WGA/Lamp1 expressing structures were observed in wild-type (OreR) guts (Fig. 6G; Fig.
493 S4F).

Katheder et al., Fig. 6



495 **Figure 6: Syt4 knockdown affects PM integrity and phenocopies nAChR depletion**

496 A) Survival after one day of mCherry (ctrl) or Syt4 depletion in ECs followed by *Pseudomonas*
497 *entomophila* infection. n=175 animals per genotype and condition; N=3. Log Rank (Mantel-Cox)
498 test.

499 B) Confocal immunofluorescence image of posterior midguts depleted for either mCherry (control)
500 or Syt4 for 8 days. Animals are expressing a GFP-brush border marker (green) and were fed red
501 fluorescent beads to assess peritrophic matrix (PM) integrity (beads appear yellow/orange due to
502 autofluorescence of beads in GFP channel). PM is labeled with WGA (white), DNA (blue) is
503 labeled with Hoechst. Yellow arrowheads indicate beads that leaked out of the PM sleeve. n=10
504 guts per genotype. N=3. Scale bar 25 μ m.

505 C) Survival of outcrossed w1118 (control) or Syt4 $^{\Delta}$ CRISPR null mutant flies after *Pseudomonas*
506 *entomophila* infection. n=75 animals per genotype and condition; N=3. Log Rank (Mantel-Cox)
507 test.

508 D) Confocal immunofluorescence image of posterior midguts of w1118 (control) or Syt4 $^{\Delta}$ animals
509 fed with red fluorescent beads to monitor PM integrity. PM is stained with WGA (white), DNA
510 (blue) is labeled with Hoechst in bottom panels. Yellow insets are shown enlarged in bottom row.
511 Yellow arrowheads indicate the presence (w1118) or absence of a clear PM boundary. Cyan
512 arrowheads indicate accumulation of WGA signal within the epithelium. n=10 guts per genotype.
513 N=3. Scale bar 25 μ m.

514 E) Survival after overexpression of Luciferase-RNAi (control) or Luciferase-RNAi together with
515 UAS-FLAG-mCherry-Syt4 for one day before *Pseudomonas entomophila* infection. n=100
516 animals per genotype and condition; N=3. Log Rank (Mantel-Cox) test.

517 F) Confocal immunofluorescence image of posterior midguts overexpressing UAS-FLAG-
518 mCherry-Syt4 (red) in enterocytes stained with WGA (white). DNA (blue) is labeled with Hoechst
519 in bottom panels. Yellow arrowheads indicate overlap between Syt4-positive vesicles and WGA
520 staining. n=8 guts. N=3. Scale bar 25 μ m.

521 G) Immunogold electron microscopy image of posterior midgut of an Oregon R wildtype animal
522 or an animal overexpressing UAS-FLAG-mCherry-Syt4 in enterocytes with NP1ts. WGA-biotin
523 (10nm gold particles) is detected in multilamellar bodies carrying membranous and amorphous
524 material. Syt4 (stained with anti-mCherry antibody, 15nm gold particles) colocalizes with these
525 structures in animals expressing the UAS-FLAG-mCherry-Syt4, while Oregon R samples are
526 devoid of anti-mCherry antibody labeling. n= 5. N=1. Scale bar 200nm.

527 H) Model: Neuronal or EE-derived Ach maintains barrier function through Syt4-mediated secretion
528 of PM components such as chitin from ECs. Disrupted Ach signaling leads to barrier dysfunction,
529 peritrophic matrix defects, dysbiosis, as well as loss of gut compartmentalization and
530 inflammation.

531 Ach, Acetylcholine; nAChR, nicotinic acetylcholine receptor; EC, enterocyte; EE,
532 enteroendocrine cell; Syt4, Synaptotagmin 4

533
534

535 **Discussion**

536

537 Our study identified 22 candidate COPD genes that disrupt barrier integrity in the fly and
538 demonstrates the utility of the genetically accessible fly to screen candidate disease
539 genes from human GWAS studies to provide mechanistic insight into their role in tissue
540 homeostasis and pathophysiology. In particular, our results provide a role for nAchR
541 signaling in maintaining intestinal barrier function. Since depletion of several nAchR
542 subunits in enterocytes, or of ChAT in neurons and EEs leads to loss of barrier integrity
543 and decreased survival after chemical or bacterial challenge, we propose that
544 acetylcholine-mediated crosstalk between cholinergic neurons and/or EEs with ECs is
545 critical to maintain intestinal epithelial homeostasis. This role of nAchR signaling is
546 mediated by transcriptional regulation of Syt4 in ECs, which in turn maintains secretion
547 of chitin vesicles to maintain the peritrophic matrix (Fig. 6H).

548 A role for acetylcholine signaling in human barrier epithelia is supported by previous
549 studies: muscarinic acetylcholine receptors have been successfully targeted in the clinic
550 to relieve bronchoconstriction and mucus hypersecretion in COPD and asthma (Calzetta
551 et al., 2021), although nicotinic AchRs remain more elusive from a therapeutic perspective
552 (Hollenhorst & Krasteva-Christ, 2021). While Ach is a classic neurotransmitter, a growing
553 body of work has uncovered an important role of Ach beyond the context of the nervous
554 system: various non-neuronal cell types express the machinery for Ach synthesis and
555 secretion, ranging from diverse immune cells to epithelial cells, such as brush/tuft cells
556 (Kummer & Krasteva-Christ, 2014; Wessler & Kirkpatrick, 2008). Airway tuft cells have
557 been implicated in orchestrating type 2 inflammatory responses (O'Leary et al., 2019; Sell
558 et al., 2021) and mucociliary clearance (Perniss et al., 2020), whereas their intestinal
559 counterparts participate in defense against helminths and protists and limit biliary
560 inflammation (O'Leary et al., 2022; O'Leary et al., 2019). With a wide range of cell types
561 able to produce or sense Ach, non-neuronal Ach serves as a versatile signaling molecule
562 eliciting complex intercellular crosstalk with diverse outcomes; depending on the context,
563 Ach may promote inflammation or conversely exert anti-inflammatory functions
564 (Hollenhorst & Krasteva-Christ, 2021; Kummer & Krasteva-Christ, 2014; Sell et al., 2021).
565 Accordingly, it was recently reported that expression of a COPD risk allele of CHRNA5 in

566 epithelial cells leads to airway remodeling *in vivo*, increased proliferation and production
567 of pro-inflammatory cytokines through decreased calcium entry and increased adenylyl-
568 cyclase activity (Routhier et al., 2021).

569 Previous work has further shown a downregulation of junctional proteins such as ZO-1
570 and p120 after depletion of CHRNA5 in A549 cells lung cancer cells (Krais et al., 2011).
571 While we observed a slightly disorganized pattern of junctional markers such as Dlg after
572 nAChR subunit knockdown in the fly intestinal epithelium, junctional architecture appeared
573 normal when analyzed by electron microscopy. Furthermore, transcriptome analysis
574 revealed little to no changes in the expression of proteins involved in polarity or cellular
575 junction formation, suggesting that nAChR signaling regulates barrier function through
576 other mechanisms. A role for the Syt4-mediated secretion of PM protein components and
577 chitin in maintaining barrier integrity is supported by the observation that mCherry-tagged
578 Syt4 partially overlaps with chitin-binding wheat germ agglutinin staining.

579 While the *Drosophila* PM is thought to be produced mostly in the anterior most portion of
580 the gut (Hegedus et al., 2019), the existence of WGA-positive vesicles throughout the
581 entire midgut suggests continuous remodeling along the length of the tissue. This finding
582 is consistent with the previously reported expression of PM-related transcripts in the R4
583 compartment of the midgut (Buchon et al., 2013). PM integrity can be modulated by
584 enteric neurons, although a role for cholinergic signaling was not tested in this context
585 (Kenmoku et al., 2016).

586 Our study highlights the evolutionary conservation of mechanisms maintaining epithelial
587 barrier function. The PM is functionally analogous to mucus and surfactant layers in
588 mammalian airways, and it remains to be explored whether COPD risk alleles in nAChR
589 subunits also cause a dysfunction in the secretion of such barrier components. The
590 elevated inflammation and airway remodeling in mice expressing the CHRNA5 risk allele
591 suggest that such a mechanism may be conserved as well (Routhier et al., 2021) . It is
592 critical to note that the epithelial dysfunction observed in these animals, as well as part of
593 the association of COPD risk with specific CHRNA loci, emerge independently of cigarette
594 smoke (Parker et al., 2019; Routhier et al., 2021; Siedlinski et al., 2013), indicating that
595 nAChR signaling is critical to maintain homeostasis not only in the context of oxidative
596 stress, but under homeostatic conditions. Supporting this view, our data show that

597 knockdown of nAchR subunits in fly ECs also results in epithelial stress signaling in the
598 absence of Paraquat exposure.

599 These consistencies further validate the approach of prioritizing candidate genes
600 associated with COPD risk loci using the *Drosophila* intestine as a model system.
601 Characterization of the epithelial role of other identified candidate orthologues from our
602 screen will likely provide further insight into the biology and pathophysiology of barrier
603 dysfunction and epithelial homeostasis. Such studies will be critical for target identification
604 and validation for therapeutic intervention in COPD.

605

606 **Material and methods**

607

608 ***Drosophila* stocks and husbandry**

609 Flies were raised and kept on standard fly food prepared according to the following recipe:

610 1 l distilled water, 13.8 g agar, 22 g molasses, 75 g malt extract, 18 g inactivated dry

611 yeast, 80 g corn flour, 10 g soy flour, 6.26 ml propionic acid, 2 g methyl 4-

612 hydroxybenzoate in 7.2 ml of ethanol. Flies were reared at 25°C with 65% humidity on a

613 12 h light/dark cycle. All animals used in this study were mated females matured for 4-6

614 days.

615 The TARGET system was used to conditionally express UAS-linked transgenes in

616 specific cell populations in combination with indicated Gal drivers (McGuire et al., 2004).

617 Crosses containing tub::Gal80^{ts} were reared at 18°C to avoid premature gene expression.

618 Transgene expression was induced by shifting the flies to 29°C for 1-8 days, as indicated

619 in the figure legends.

620 For experiments using a GeneSwitch driver, flies were reared on normal food before

621 being shifted to food containing 200mM Mifepristone (RU486); for barrier function

622 experiments (smurf assay). FD&C blue dye (Neta Scientific, SPCM-FD110-04) was

623 added to the food at final concentration of 2.5% (w/v).

624 Formation of MARCM clones was induced with heat shock for 1h at 37°C and clones

625 were analyzed after 7 days at 25°C.

626 RNAi lines used in the barrier dysfunction screen are listed in Suppl Fig. 1B.

627 The following additional lines were obtained from the Bloomington *Drosophila* Stock

628 Center: w¹¹¹⁸, Oregon-R, UAS-mCherry^{RNAi} (35785), UAS-ChAT^{RNAi} (60028, 25856),

629 FRT82B (2051), w*; TI{TI}nAChR α 2attP/TM6B (84540), w[*]; Mi{Trojan-

630 GAL4.0}ChAT[MI04508-TG4.0] CG7715[MI04508-TG4.0-X]/TM6B (60317)

631 The following additional lines were obtained from the Vienna *Drosophila* Stock Center:

632 UAS-nAchR β 1^{RNAi} (33825, pruned), UAS-nAchR β 3^{RNAi} (42742, pruned), UAS-

633 ChAT^{RNAi}(20183, 330291).

634 The following lines were gifts: 5966::GeneSwitch (B. Ohlstein), 2xSTAT::GFP (E. Bach),
635 NP1::Gal4 (D. Ferrandon), A142::GFP (N. Buchon), Mex1::Gal4;tub::G80ts (L. O'Brien),
636 MARCM82 (hsFlp; tub::Gal4, UAS::GFP; FRT82, tub::Gal80, Norbert Perrimon),
637 ProsV1::Gal4 (PMID: 11486507), Da::GeneSwitch (PMID: 19486910), UAS::Xbp1-eGFP
638 (H. D. Ryoo)

639

640 **Generation of UAS-ChAT**

641 DNA encoding the sequence of Choline O-acetyltransferase (Uniprot identifier P07668,
642 amino acid residues 1-721), was synthesized and subcloned into pUASTattB under the
643 control of the hsp70 promoter. Transgenic lines were established by WellGenetics,
644 Taiwan. In brief, pUASTattB plasmid containing the ChAT sequence was microinjected
645 into embryos of y[1] M{vas-int.Dm}ZH-2A w[*]; P{y[+t7.7]=CaryP}attP40 or y[1] M{vas-
646 int.Dm}ZH-2A w[*]; P{y[+t7.7]=CaryP}attP2. Transgenic F1 flies were screened for the
647 selection marker white+ (orange colored eyes).

648

649 **Syt4 CRISPR mutant**

650 CRISPR mediated mutagenesis was performed by WellGenetics, Inc. (Taiwan) using
651 modified methods of Kondo and Ueda (Kondo & Ueda, 2013). In brief, the upstream gRNA
652 sequences TTTCCACTCGATGTTCTGG[CGG] and downstream gRNA sequences
653 CGCAGGCGCCCCCTTAATGAG[GGG] were cloned into U6 promoter plasmids
654 separately. Cassette 3xP3 RFP, which contains a floxed 3xP3 RFP and two homology
655 arms, were cloned into pUC57 Kan as donor template for repair. Syt4/CG10047- targeting
656 gRNAs and hs Cas9 were supplied in DNA plasmids, together with donor plasmid for
657 microinjection into embryos of control strain w[1118]. F1 flies carrying the selection
658 marker 3xP3 RFP were further validated by genomic PCR and sequencing. This CRISPR
659 editing generates a 2,603 bp deletion allele of Syt4, deleting the entire CDS and replacing
660 it with a 3xP3 RFP cassette.

661

662 **Gene assignment to COPD genome-wide association study (GWAS) loci**

663 Publicly available summary statistics for the discovery stage of the COPD GWAS reported
664 by Hobbs *et al.*, 2017 were obtained from dbGaP (accession: phs000179). Forty-eight
665 candidate genes were assigned to the 22 loci reported in Hobbs *et al.*, 2017 based upon
666 expression quantitative trait loci (eQTL), coding variation level support or physical
667 distance if a gene could not be assigned via the former criteria. First, candidate genes
668 were assigned to loci if the index variant was an eQTL in any tissue for any gene within
669 250 kilobases of the variant in GTEx (Battle *et al.*, 2017) (V6p). We further applied
670 colocalization (via the coloc package in R) (Giambartolomei *et al.*, 2014) to estimate the
671 probability the eQTL and COPD risk association signal share a causal variant. Of the 40
672 genes with eQTL support, 24 had a colocalization probability > 0.6 . Candidate genes were
673 also assigned to loci if the index variant was in linkage disequilibrium (LD) ($r^2 > 0.6$) with
674 coding variants for the gene. LD was estimated using individuals of European ancestry
675 from 1000 Genomes (Auton *et al.*, 2015). Eight candidate genes were assigned to five
676 loci, six of which overlapped genes with eQTL level support.

677 Since we first obtained this candidate gene list, a larger COPD risk GWAS was published
678 (Sakornsakolpat *et al.*, 2019) that made use of not only lung eQTL and coding variant
679 data, but also epigenetic and gene-set similarity approaches to assign candidate genes
680 to COPD risk loci (see Supplementary Table 7 in Sakornsakolpat *et al.*, 2019). We found
681 our assigned candidate genes overlapped with candidate genes from this newer study at
682 13/22 loci reported in the Hobbs *et al.*, 2017 study, including CHRNA3/5. Overall 20/48
683 candidate genes were also listed as candidate genes in the Sakornsakolpat *et al.* study.

684

685 **Barrier Dysfunction Screen**

686 For the barrier dysfunction assay, males from candidate RNAi lines were crossed at a 1:1
687 ratio with virgin *Daughterless* (*Da*)::GeneSwitch driver line females in Bloomington-
688 modified food (standard medium) bottles. Crosses were raised at 25°C and brooded every
689 2-3 days. Progeny were collected and females were sorted after mating for 2-3 days
690 (discarding males). This yielded about 200 females per genotype depending on the RNAi
691 line. Sorted females were aged in standard medium at 25°C for 10-12 days. Aged females
692 (~25 per vial; exact number recorded per vial for assay read-out) were then exposed to

693 standard medium prepared with 200mM Mifepristone (RU486) from Sigma Aldrich (cat#
694 856177) and 2.5% w/v FD&C Blue Dye no 1 from Spectrum (cat# FD110) for 24 hours at
695 25°C or 29°C. Prior to paraquat exposure, flies were dry starved for 2-3 hours at the
696 experimental temperature. 25mM paraquat solution (5% sucrose and 2.5% w/v FD&C
697 Blue Dye in sterile water) or mock solution (sucrose and blue dye only) was freshly
698 prepared for each experiment.. Starved flies were placed in empty vials with a Whatman
699 filter paper (VWR, 89013-946) on top of a foam biopsy pad (Neta Sciences, BPLS-6110)
700 and 1.25mL of paraquat or mock solution for 16 hours at 25°C or 29°C and then shifted
701 back to medium with 200mM Mifepristone (RU486) and 2.5% w/v FD&C Blue Dye no 1.
702 Entirely Blue (Smurf) flies were counted starting post-16-hour exposure. Smurf flies were
703 counted daily or every-other day. About 8-12 candidate RNAi lines were tested in sets
704 with Luciferase RNAi always included as a control.

705 The average proportion of smurf flies across technical replicates per time point were
706 calculated and graphed. The natural log (LN) ratio was calculated for each candidate
707 RNAi by dividing the candidate RNAi proportion average from the final time point by the
708 luciferase RNAi proportion average for the same time point (=LN(Candidate
709 RNAi/Luciferase RNAi)). Candidate RNAi results were ranked by establishing a scale with
710 arbitrary LN ratio ranges to define: strong enhancers (≥ 1), enhancers (≥ 0.43 to ≤ 0.99),
711 weak enhancers (≥ 0.20 to ≤ 0.42), no effect (≥ -0.30 to ≤ 0.19), weak suppressors ($\geq -$
712 0.70 to ≤ -0.31), suppressors (≥ -1.10 to ≤ -0.71), and strong suppressors (≤ -1.11).

713

714 **Paraquat feeding**

715 20-25 flies per vial were kept on food containing FD&C blue for 1-3 days and dry starved
716 in empty vials for 2-3h prior to Paraquat exposure. Methyl viologen dichloride hydrate
717 (Paraquat, 856177, Sigma Aldrich) solution was prepared freshly for each experiment in
718 5% (w/v) sucrose in water with 2% (w/v) FD&C blue. Paraquat concentration was 12.5mM
719 unless indicated otherwise. Starved flies were transferred to vials containing 600 μ l of
720 Paraquat solution or 5% sucrose (mock treatment) as well as a circular Whatman filter
721 paper (VWR, 89013-946) on top of a foam biopsy pad (Neta Sciences, BPLS-6110). Flies
722 were treated for 16h overnight and then transferred back to fly food with FD&C blue dye.

723 The number of smurf flies was recorded 24h after the start of the Paraquat challenge and
724 subsequently monitored over the course of 7-10 days.

725

726 ***Pseudomonas entomophila* infection**

727 *Pseudomonas entomophila* (PE, gift from B. Lemaitre), was cultured in LB medium at
728 29 °C overnight for 16-18h (15ml/sample to be infected). Bacteria were centrifuged at
729 4000g for 10 min at RT and resuspended in 5% sucrose (OD₆₀₀=100). 500µl of
730 concentrated bacterial suspension or 5% (w/v) sucrose solution (mock treatment) was
731 added to empty fly vials containing a circular Whatman filter paper (VWR, 89013-946) on
732 top of a foam biopsy pad (Neta Sciences, BPLS-6110). 20-25 flies per vial were starved
733 in empty vials for 2–3 h before infection. Survival was monitored over the course of 7-10
734 days and 100µl of sucrose solution was added daily.

735

736 **Gut compartmentalization**

737 Gut compartmentalization was assessed as described in Li et al., 2016: 100µl of 2% w/v
738 Bromphenol blue solution (Sigma Aldrich, B5525) was dispensed in a food vial, the
739 surface was broken up with a pipette tip to allow full absorption of the dye before flies
740 were transferred onto food. Flies were fed overnight and guts were dissected in small
741 groups and immediately scored visually under a stereomicroscope to avoid prolonged
742 exposure to CO₂.

743

744 **Immunofluorescence microscopy**

745 Guts from adult female flies were dissected in PBS, fixed for 45mins at room temperature
746 (RT) in fixative solution (4% formaldehyde, 100 mM glutamic acid, 25 mM KCl, 20 mM
747 MgSO₄, 4 mM Na₂HPO₄, 1 mM MgCl₂, pH 7.5), washed twice in wash buffer (1× PBS,
748 0.5% bovine serum albumin and 0.1% Triton X-100, 0.005% NaN₃) for 30 min at RT.
749 Primary and secondary antibodies were diluted in wash buffer. Samples were incubated
750 overnight at 4°C with primary antibody, washed twice for 30min with wash buffer before
751 incubating 4-6h at RT with secondary antibody. Hoechst33342 (Invitrogen, H3570,

752 1:1000) or wheat germ agglutinin-AlexaFluor647 (Invitrogen, W32466, 1:500) were added
753 to the secondary antibody cocktail to visualize DNA or the peritrophic matrix (PM)
754 respectively. Samples were washed again twice for 30mins before mounting in Prolong
755 Glass antifade mounting media (Invitrogen, P36982).

756 To assess the integrity of the PM, flies were dry starved for 2h and then fed Fluoresbrite
757 microspheres (Polysciences, 17149 (0.05µm, green) or 195075 (0.5µm, red), diluted 1:50
758 in 5% sucrose solution on Whatman filter paper for 16h overnight. Guts were dissected,
759 fixed and processed for immunofluorescence microscopy analysis as described above.

760 For lysotracker staining, freshly dissected guts were incubated for 5mins in 1× PBS with
761 Lysotracker Deep Red (Invitrogen, L12492, 1:500) before fixation. Samples were washed
762 twice for 10mins before and after 1h incubation with Hoechst, mounted and analyzed
763 within one day.

764 Primary antibodies used in this study: chicken anti-GFP (Abcam, ab13970, 1:1000),
765 mouse anti-armadillo (DSHB, N2 7A1, 1:100), mouse anti-Delta (DSHB, C594.9B, 1:50),
766 mouse anti-Dlg (DSHB, 4F3 anti-discs large, 1:20), mouse anti-ChAT (DSHB, ChAT4B1,
767 1:100), rabbit anti-phospho Histone H3 (Millipore, 06-570, 1:2000), mouse anti-prospero
768 (DSHB, MR1A, 1:250), mouse anti-cut (DSHB, 2B10, 1:100), mouse anti-Golgin84
769 (DSHB, Golgin 84 12-1, neat)

770 Secondary antibodies were from Jackson ImmunoResearch Laboratories and diluted
771 1:1000. donkey anti-mouse Cy3 (Jackson ImmunoResearch Laboratories, 715-165-150,
772 1:1000), donkey anti-mouse Alexa-647 (Invitrogen, A31571, 1:1000), donkey anti-chicken
773 Alexa-488 (Jackson ImmunoResearch Laboratories, 703-545-155, 1:1000), donkey anti-
774 rabbit Cy3 (Jackson ImmunoResearch Laboratories, 711-165-152, 1:1000), donkey anti-
775 rabbit Alexa 647 (Jackson ImmunoResearch Laboratories, 711-605-152, 1:1000)

776 All Images were taken on a Leica SP8 confocal microscope and processed using
777 FIJI(Schindelin et al., 2012) and Adobe Illustrator.

778

779 **CFU counting**

780 Commensal bacteria were cultured as described in (Guo et al., 2014):. In brief, intact flies
781 were sanitized in 70% ethanol for 1min and rinsed 3x in sterile PBS. 5 guts per sample
782 were dissected and homogenized in 250 μ l sterile PBS. Serial dilutions were plated on
783 selective media, plates were incubated for 48-72h at 29°C and colonies counted.

784 Selective plates were prepared according to the following recipes: *Acetobacteriaceae*: 25
785 g/l D-mannitol, 5 g/l yeast extract, 3 g/l peptone, and 15 g/l agar. *Enterobacteriaceae*: 10
786 g/l Tryptone, 1.5 g/l yeast extract, 10 g/l glucose, 5 g/l sodium chloride, 12 g/l agar.
787 *Lactobacilli* MRS agar: 70 g/l BD Difco Lactobacilli MRS agar. *Nutrient Rich Broth*: 23 g/l
788 BD Difco Nutrient agar. All media were autoclaved at 121 degrees Celsius for 15 min.

789

790 **Electron microscopy (EM)**

791 For the localization of Syt4, flies were allowed to express UAS-3xFLAG-mCherry-Syt4
792 in enterocytes under control of NP1ts for 2 days before dissection in PBS at room
793 temperature. The dissected gut was cut with a sharp blade at the R3-R4 border and the
794 R4-hindgut segment was immediately immersed in either one of 2 fixative solutions, to
795 obtain samples for immuno-EM and for conventional EM in Epon-embedded material.

796 For immuno-EM (Slot & Geuze, 2007), the fixation was performed with 4%
797 paraformaldehyde (PFA), 0.1% glutaraldehyde (GA) in PHEM buffer (60mM PIPES, 25
798 mM HEPES, 2 mM MgCl₂, 10 mM EGTA), pH 6.9, for 1h at room temperature.

799 Subsequently, fixation was continued in 0.6 % PFA in PHEM buffer at 4 °C for several
800 days. The samples were then rinsed in PBS, blocked with 0.15 % glycine in PBS, and
801 gradually embedded in gelatin, from 2% (30 min) over 6% (30 min) to 12 % gelatin.

802 Small blocks of solidified gelatin each containing 1 gut segment were cryoprotected
803 overnight with 2.3 M sucrose. They were mounted on aluminum pins in a direction to
804 expose the transversal cut at the R4 segment for cryo-ultramicrotomy and frozen in
805 liquid N2. Syt4 was localized on ultrathin cryosections with polyclonal rabbit anti-RFP
806 antibody (600-401-379, Rockland). Chitin was localized with biotinylated wheat germ
807 agglutinin (B-1025-5, Vector laboratories) followed by polyclonal rabbit anti-biotin
808 antibody (100-4198, Rockland). *Drosophila*-specific rabbit anti-Lamp1 antibody was a
809 gift from Andreas Jenny (Chaudhry et al., 2022). Antibodies were detected with protein

810 A -conjugated with 15 or 10 nm gold particles in a JEOL JEM-1011 electron
811 microscope.
812 For conventional EM the fixation was performed in 2.5 % GA in 0.1 M Sorensen's
813 phosphate buffer (PB), pH 7.4, for 4 h at room temperature, then overnight at 4 °C.
814 Subsequently, fixation was continued in 0.6 % PFA in 0.1 M PB at 4 °C for several days.
815 After rinsing in 0.1 M PB, the guts were postfixed with 1 % OsO₄ and 1.5 % K₃[Fe(CN)₆]
816 in 0.07 M PB, stained en bloc in aqueous 0.5 % uranyl acetate, dehydrated in acetone
817 and embedded in Epon. Transverse sections of the R4 gut segments were stained with
818 uranyl acetate and lead citrate and examined in a JEOL JEM-1011 electron microscope.
819

820 **Bulk RNAseq**

821 For bulk RNAseq analysis 4 independent biological replicates per sample consisting of
822 20-25 guts each were dissected and collected on dry ice. RNA was extracted using the
823 Qiagen RNeasy Mini kit.

824 cDNA was generated from 2 ng of RNA using the Smart-Sq V4 Ultra Low Input RNA Kit
825 (Takara, 634894). Next, 150 pg of cDNA was used to produce sequencing libraries with
826 the Nextera XT DNA Sample Preparation Kit (Illumina, FC-131-1024). Libraries were then
827 sequenced for 50 single read cycles and 30 million reads per sample on Illumina NovaSeq
828 6000. Reads were aligned to the *Drosophila* genome, version BDGP6, using the GSNAP
829 aligner as part of the HTSeqGenie R package (version 4.2). Reads that uniquely aligned
830 within exonic boundaries of genes were used to derive expression estimates. nRPKM
831 values, in which total library sizes were normalized using the median ratio method as
832 previously described (Anders & Huber, 2010), were generated for each gene. Partek Flow
833 was used to perform differential gene expression and PCA analysis, gene ontology term
834 enrichment as well as creation of illustrative graphs.

835

836 **Statistical analyses**

837 Generation of graphs and statistical analyses were performed with Graphpad Prism 9.

838 Experiments with two conditions were compared with a two-tailed parametric Student's
839 T-test or Fischer's exact test, as appropriate. Experiments with multiple conditions were
840 evaluated either by ordinary one-way ANOVA followed by Dunnett's post-hoc test to
841 compare a control group with experimental conditions or a Chi square test for categorical
842 data. Barrier dysfunction curves were analyzed with 2-way ANOVA followed by Sidak's
843 multiple comparisons test. Survival curves were compared with the Mantel-Cox method.
844 No statistical methods were used to predetermine sample sizes; sample sizes were
845 determined based on variation observed in pilot experiments and previously published
846 literature. Exact numbers are listed in figure legends. All animals were randomly allocated
847 to treatment groups. The experimenter was blinded for image analysis and other
848 quantifications. The number of repeats for each experiment is listed in figure legends, all
849 attempts at replication were successful. The initial screen as well as electron microscopy
850 and RNAseq experiments were performed once for data gathering and hypothesis
851 generation; the data was later validated by other methods. No data points were excluded
852 from analyses.

853

854 **Illustrative model**

855 Illustrative model summarizing results was created with BioRender.com

856

857 **Data availability**

858 All data generated and analyzed are included in the manuscript, figures and figure
859 supplements. All sequencing data generated in this study will be deposited in GEO
860 under accession code XX and XX.

861

862 **Illustrative model**

863 Illustrative model summarizing results was created with BioRender.com

864

865 **Material availability**

866 Fly lines generated in this study (UAS-ChAT and Syt4 CRISPR mutant) are available
867 upon request.

868

869 **Adherence to community standards**

870 This study and manuscript were prepared in accordance with ARRIVE and ICMJE
871 guidelines.

872

873 **Acknowledgements**

874 We thank Dr Andreas Jenny (Albert Einstein College of Medicine) for the *Drosophila*-
875 specific rabbit anti-Lamp1 antibody.

876 We thank Dr Aniek Janssen and Dr Lucie van Leeuwen (UMC Utrecht) for the Oregon R
877 flies for EM.

878

879 The microscopy infrastructure in this work is subsidized by the Roadmap for Large-
880 Scale Research Infrastructure (NEMI) of Netherlands Organisation for Scientific
881 Research (grant number 184.034.014 to J.K.).

882

883

884 **References**

885 Aghapour, M., Raee, P., Moghaddam, S. J., Hiemstra, P. S., & Heijink, I. H. (2018). Airway
886 Epithelial Barrier Dysfunction in Chronic Obstructive Pulmonary Disease: Role of Cigarette
887 Smoke Exposure. *Am J Respir Cell Mol Biol*, 58(2), 157-169.
888 <https://doi.org/10.1165/rcmb.2017-0200TR>

889 Aghapour, M., Ubags, N. D., Bruder, D., Hiemstra, P. S., Sidhaye, V., Rezaee, F., & Heijink, I. H.
890 (2022). Role of air pollutants in airway epithelial barrier dysfunction in asthma and COPD.
891 *Eur Respir Rev*, 31(163). <https://doi.org/10.1183/16000617.0112-2021>

892 Amos, C. I., Wu, X., Broderick, P., Gorlov, I. P., Gu, J., Eisen, T., Dong, Q., Zhang, Q., Gu, X.,
893 Vijayakrishnan, J., Sullivan, K., Matakidou, A., Wang, Y., Mills, G., Doheny, K., Tsai, Y.,
894 Y., Chen, W. V., Shete, S., Spitz, M. R., & Houlston, R. S. (2008). Genome-wide
895 association scan of tag SNPs identifies a susceptibility locus for lung cancer at 15q25.1.
896 *Nat Genet*, 40(5), 616-622. <https://doi.org/10.1038/ng.109>

897 Anders, S., & Huber, W. (2010). Differential expression analysis for sequence count data.
898 *Genome Biol*, 11(10), R106. <https://doi.org/10.1186/gb-2010-11-10-r106>

899 Auton, A., Brooks, L. D., Durbin, R. M., Garrison, E. P., Kang, H. M., Korbel, J. O., Marchini, J. L.,
900 McCarthy, S., McVean, G. A., & Abecasis, G. R. (2015). A global reference for human
901 genetic variation. *Nature*, 526(7571), 68-74. <https://doi.org/10.1038/nature15393>

902 Bach, E. A., Ekas, L. A., Ayala-Camargo, A., Flaherty, M. S., Lee, H., Perrimon, N., & Baeg, G.
903 H. (2007). GFP reporters detect the activation of the Drosophila JAK/STAT pathway in
904 vivo. *Gene Expr Patterns*, 7(3), 323-331. <https://doi.org/10.1016/j.modgep.2006.08.003>

905 Barnes, P. J. (2019). Inflammatory endotypes in COPD. *Allergy*, 74(7), 1249-1256.
906 <https://doi.org/10.1111/all.13760>

907 Battle, A., Brown, C. D., Engelhardt, B. E., & Montgomery, S. B. (2017). Genetic effects on gene
908 expression across human tissues. *Nature*, 550(7675), 204-213.
909 <https://doi.org/10.1038/nature24277>

910 Biteau, B., Hochmuth, C. E., & Jasper, H. (2008). JNK activity in somatic stem cells causes loss
911 of tissue homeostasis in the aging Drosophila gut. *Cell Stem Cell*, 3(4), 442-455.
912 <https://doi.org/10.1016/j.stem.2008.07.024>

913 Biteau, B., Hochmuth, C. E., & Jasper, H. (2011). Maintaining tissue homeostasis: dynamic
914 control of somatic stem cell activity. *Cell Stem Cell*, 9(5), 402-411.
915 <https://doi.org/10.1016/j.stem.2011.10.004>

916 Buchon, N., Broderick, N. A., Chakrabarti, S., & Lemaitre, B. (2009). Invasive and indigenous
917 microbiota impact intestinal stem cell activity through multiple pathways in Drosophila.
918 *Genes Dev*, 23(19), 2333-2344. <https://doi.org/10.1101/gad.1827009>

919 Buchon, N., Broderick, N. A., Poidevin, M., Pradervand, S., & Lemaitre, B. (2009). Drosophila
920 intestinal response to bacterial infection: activation of host defense and stem cell
921 proliferation. *Cell Host Microbe*, 5(2), 200-211.
922 <https://doi.org/10.1016/j.chom.2009.01.003>

923 Buchon, N., Osman, D., David, F. P., Fang, H. Y., Boquete, J. P., Deplancke, B., & Lemaitre, B.
924 (2013). Morphological and molecular characterization of adult midgut
925 compartmentalization in Drosophila. *Cell Rep*, 3(5), 1725-1738.
926 <https://doi.org/10.1016/j.celrep.2013.04.001>

927 Caliri, A. W., Tommasi, S., & Besaratinia, A. (2021). Relationships among smoking, oxidative
928 stress, inflammation, macromolecular damage, and cancer. *Mutat Res Rev Mutat Res*,
929 787, 108365. <https://doi.org/10.1016/j.mrrev.2021.108365>

930 Calzetta, L., Coppola, A., Ritondo, B. L., Matino, M., Chetta, A., & Rogliani, P. (2021). The Impact
931 of Muscarinic Receptor Antagonists on Airway Inflammation: A Systematic Review. *Int J*
932 *Chron Obstruct Pulmon Dis*, 16, 257-279. <https://doi.org/10.2147/COPD.S285867>

933 Carlier, F. M., de Fays, C., & Pilette, C. (2021). Epithelial Barrier Dysfunction in Chronic
934 Respiratory Diseases. *Front Physiol*, 12, 691227.
<https://doi.org/10.3389/fphys.2021.691227>

935 Carlini, C. R., & Grossi-de-Sá, M. F. (2002). Plant toxic proteins with insecticidal properties. A
936 review on their potentialities as bioinsecticides. *Toxicon*, 40(11), 1515-1539.
[https://doi.org/10.1016/s0041-0101\(02\)00240-4](https://doi.org/10.1016/s0041-0101(02)00240-4)

937 Chaudhry, N., Sica, M., Surabhi, S., Hernandez, D. S., Mesquita, A., Selimovic, A., Riaz, A.,
938 Lescat, L., Bai, H., MacIntosh, G. C., & Jenny, A. (2022). Lamp1 mediates lipid transport,
939 but is dispensable for autophagy in Drosophila. *Autophagy*, 18(10), 2443-2458.
<https://doi.org/10.1080/15548627.2022.2038999>

940 Cognigni, P., Bailey, A. P., & Miguel-Aliaga, I. (2011). Enteric neurons and systemic signals
941 couple nutritional and reproductive status with intestinal homeostasis. *Cell Metab*, 13(1),
942 92-104. <https://doi.org/10.1016/j.cmet.2010.12.010>

943 Cui, K., Ge, X., & Ma, H. (2014). Four SNPs in the CHRNA3/5 alpha-neuronal nicotinic
944 acetylcholine receptor subunit locus are associated with COPD risk based on meta-
945 analyses. *PLoS One*, 9(7), e102324. <https://doi.org/10.1371/journal.pone.0102324>

946 De Gregorio, E., Spellman, P. T., Tzou, P., Rubin, G. M., & Lemaitre, B. (2002). The Toll and Imd
947 pathways are the major regulators of the immune response in Drosophila. *Embo J*, 21(11),
948 2568-2579. <https://doi.org/10.1093/emboj/21.11.2568>

949 Deng, B., Li, Q., Liu, X., Cao, Y., Li, B., Qian, Y., Xu, R., Mao, R., Zhou, E., Zhang, W., Huang,
950 J., & Rao, Y. (2019). Chemoconnectomics: Mapping Chemical Transmission in
951 Drosophila. *Neuron*, 101(5), 876-893.e874. <https://doi.org/10.1016/j.neuron.2019.01.045>

952 Dubreuil, R. R. (2004). Copper cells and stomach acid secretion in the Drosophila midgut. *Int J
953 Biochem Cell Biol*, 36(5), 745-752. <https://doi.org/10.1016/j.biocel.2003.07.004>

954 Erlandson, M. A., Toprak, U., & Hegedus, D. D. (2019). Role of the peritrophic matrix in insect-
955 pathogen interactions. *J Insect Physiol*, 117, 103894.
<https://doi.org/10.1016/j.jinsphys.2019.103894>

956 Giambartolomei, C., Vukcevic, D., Schadt, E. E., Franke, L., Hingorani, A. D., Wallace, C., &
957 Plagnol, V. (2014). Bayesian test for colocalisation between pairs of genetic association
958 studies using summary statistics. *PLoS Genet*, 10(5), e1004383.
<https://doi.org/10.1371/journal.pgen.1004383>

959 Guo, L., Karpac, J., Tran, S. L., & Jasper, H. (2014). PGRP-SC2 promotes gut immune
960 homeostasis to limit commensal dysbiosis and extend lifespan. *Cell*, 156(1-2), 109-122.
<https://doi.org/10.1016/j.cell.2013.12.018>

961 Hegedus, D., Erlandson, M., Gillott, C., & Toprak, U. (2009). New insights into peritrophic matrix
962 synthesis, architecture, and function. *Annu Rev Entomol*, 54, 285-302.
<https://doi.org/10.1146/annurev.ento.54.110807.090559>

963 Hegedus, D. D., Toprak, U., & Erlandson, M. (2019). Peritrophic matrix formation. *J Insect Physiol*,
964 117, 103898. <https://doi.org/10.1016/j.jinsphys.2019.103898>

965 Hobbs, B. D., de Jong, K., Lamontagne, M., Bossé, Y., Shrine, N., Artigas, M. S., Wain, L. V.,
966 Hall, I. P., Jackson, V. E., Wyss, A. B., London, S. J., North, K. E., Franceschini, N.,
967 Strachan, D. P., Beaty, T. H., Hokanson, J. E., Crapo, J. D., Castaldi, P. J., Chase, R. P.,
968 ... Cho, M. H. (2017). Genetic loci associated with chronic obstructive pulmonary disease
969 overlap with loci for lung function and pulmonary fibrosis. *Nat Genet*, 49(3), 426-432.
<https://doi.org/10.1038/ng.3752>

970 Hollenhorst, M. I., & Krasteva-Christ, G. (2021). Nicotinic Acetylcholine Receptors in the
971 Respiratory Tract. *Molecules*, 26(20). <https://doi.org/10.3390/molecules26206097>

972 Hu, Y., Flockhart, I., Vinayagam, A., Bergwitz, C., Berger, B., Perrimon, N., & Mohr, S. E. (2011).
973 An integrative approach to ortholog prediction for disease-focused and other functional
974 studies. *BMC Bioinformatics*, 12, 357. <https://doi.org/10.1186/1471-2105-12-357>

983 Hung, R. J., McKay, J. D., Gaborieau, V., Boffetta, P., Hashibe, M., Zaridze, D., Mukeria, A.,
984 Szeszenia-Dabrowska, N., Lissowska, J., Rudnai, P., Fabianova, E., Mates, D., Bencko,
985 V., Foretova, L., Janout, V., Chen, C., Goodman, G., Field, J. K., Liloglou, T., . . . Brennan,
986 P. (2008). A susceptibility locus for lung cancer maps to nicotinic acetylcholine receptor
987 subunit genes on 15q25. *Nature*, 452(7187), 633-637.
988 <https://doi.org/10.1038/nature06885>

989 Imler, J. L., & Bulet, P. (2005). Antimicrobial peptides in Drosophila: structures, activities and gene
990 regulation. *Chem Immunol Allergy*, 86, 1-21. <https://doi.org/10.1159/000086648>

991 Jasper, H. (2020). Intestinal Stem Cell Aging: Origins and Interventions. *Annu Rev Physiol*, 82,
992 203-226. <https://doi.org/10.1146/annurev-physiol-021119-034359>

993 Jiang, H., Patel, P. H., Kohlmaier, A., Grenley, M. O., McEwen, D. G., & Edgar, B. A. (2009).
994 Cytokine/Jak/Stat signaling mediates regeneration and homeostasis in the Drosophila
995 midgut. *Cell*, 137(7), 1343-1355. <https://doi.org/10.1016/j.cell.2009.05.014>

996 Kenmoku, H., Ishikawa, H., Ote, M., Kuraishi, T., & Kurata, S. (2016). A subset of neurons controls
997 the permeability of the peritrophic matrix and midgut structure in Drosophila adults. *J Exp
998 Biol*, 219(Pt 15), 2331-2339. <https://doi.org/10.1242/jeb.122960>

999 Kondo, S., & Ueda, R. (2013). Highly improved gene targeting by germline-specific Cas9
1000 expression in Drosophila. *Genetics*, 195(3), 715-721.
1001 <https://doi.org/10.1534/genetics.113.156737>

1002 Krais, A. M., Hautefeuille, A. H., Cros, M. P., Krutovskikh, V., Tournier, J. M., Birembaut, P.,
1003 Thépot, A., Paliwal, A., Herceg, Z., Boffetta, P., Brennan, P., & Hainaut, P. L. (2011).
1004 CHRNA5 as negative regulator of nicotine signaling in normal and cancer bronchial cells:
1005 effects on motility, migration and p63 expression. *Carcinogenesis*, 32(9), 1388-1395.
1006 <https://doi.org/10.1093/carcin/bgr090>

1007 Kummer, W., & Krasteva-Christ, G. (2014). Non-neuronal cholinergic airway epithelium biology.
1008 *Curr Opin Pharmacol*, 16, 43-49. <https://doi.org/10.1016/j.coph.2014.03.001>

1009 Kuraishi, T., Binggeli, O., Opota, O., Buchon, N., & Lemaitre, B. (2011). Genetic evidence for a
1010 protective role of the peritrophic matrix against intestinal bacterial infection in Drosophila
1011 melanogaster. *Proc Natl Acad Sci U S A*, 108(38), 15966-15971.
1012 <https://doi.org/10.1073/pnas.1105994108>

1013 Lee, T., & Luo, L. (2001). Mosaic analysis with a repressible cell marker (MARCM) for Drosophila
1014 neural development. *Trends Neurosci*, 24(5), 251-254. [https://doi.org/10.1016/s0166-2236\(00\)01791-4](https://doi.org/10.1016/s0166-
1015 2236(00)01791-4)

1016 Li, H., Qi, Y., & Jasper, H. (2016). Preventing Age-Related Decline of Gut Compartmentalization
1017 Limits Microbiota Dysbiosis and Extends Lifespan. *Cell Host Microbe*, 19(2), 240-253.
1018 <https://doi.org/10.1016/j.chom.2016.01.008>

1019 Lu, W., Liu, Z., Fan, X., Zhang, X., Qiao, X., & Huang, J. (2022). Nicotinic acetylcholine receptor
1020 modulator insecticides act on diverse receptor subtypes with distinct subunit compositions.
1021 *PLoS Genet*, 18(1), e1009920. <https://doi.org/10.1371/journal.pgen.1009920>

1022 McGuire, S. E., Mao, Z., & Davis, R. L. (2004). Spatiotemporal gene expression targeting with the
1023 TARGET and gene-switch systems in Drosophila. *Sci STKE*, 2004(220), pl6.
1024 <https://doi.org/10.1126/stke.2202004pl6>

1025 Miguel-Aliaga, I., Jasper, H., & Lemaitre, B. (2018). Anatomy and Physiology of the Digestive
1026 Tract of Drosophila melanogaster. *Genetics*, 210(2), 357-396.
1027 <https://doi.org/10.1534/genetics.118.300224>

1028 O'Leary, C. E., Sbierski-Kind, J., Kotas, M. E., Wagner, J. C., Liang, H. E., Schroeder, A. W., de
1029 Tenorio, J. C., von Moltke, J., Ricardo-Gonzalez, R. R., Eckalbar, W. L., Molofsky, A. B.,
1030 Schneider, C., & Locksley, R. M. (2022). Bile acid-sensitive tuft cells regulate biliary
1031 neutrophil influx. *Sci Immunol*, 7(69), eabj1080.
1032 <https://doi.org/10.1126/sciimmunol.abj1080>

1033 O'Leary, C. E., Schneider, C., & Locksley, R. M. (2019). Tuft Cells-Systemically Dispersed
1034 Sensory Epithelia Integrating Immune and Neural Circuitry. *Annu Rev Immunol*, 37, 47-
1035 72. <https://doi.org/10.1146/annurev-immunol-042718-041505>

1036 Parker, M. M., Lutz, S. M., Hobbs, B. D., Busch, R., McDonald, M. N., Castaldi, P. J., Beaty, T.
1037 H., Hokanson, J. E., Silverman, E. K., & Cho, M. H. (2019). Assessing pleiotropy and
1038 mediation in genetic loci associated with chronic obstructive pulmonary disease. *Genet
1039 Epidemiol*, 43(3), 318-329. <https://doi.org/10.1002/gepi.22192>

1040 Perniss, A., Liu, S., Boonen, B., Keshavarz, M., Ruppert, A. L., Timm, T., Pfeil, U., Soultanova,
1041 A., Kusumakshi, S., Delventhal, L., Aydin, Ö., Pyrski, M., Deckmann, K., Hain, T., Schmidt,
1042 N., Ewers, C., Günther, A., Lochnit, G., Chubanov, V., . . . Kummer, W. (2020).
1043 Chemosensory Cell-Derived Acetylcholine Drives Tracheal Mucociliary Clearance in
1044 Response to Virulence-Associated Formyl Peptides. *Immunity*, 52(4), 683-699.e611.
1045 <https://doi.org/10.1016/j.jimmuni.2020.03.005>

1046 Pillai, S. G., Ge, D., Zhu, G., Kong, X., Shianna, K. V., Need, A. C., Feng, S., Hersh, C. P., Bakke,
1047 P., Gulsvik, A., Ruppert, A., Lødrup Carlsen, K. C., Roses, A., Anderson, W., Rennard, S.
1048 I., Lomas, D. A., Silverman, E. K., & Goldstein, D. B. (2009). A genome-wide association
1049 study in chronic obstructive pulmonary disease (COPD): identification of two major
1050 susceptibility loci. *PLoS Genet*, 5(3), e1000421.
1051 <https://doi.org/10.1371/journal.pgen.1000421>

1052 Raftery, A. L., Tsantikos, E., Harris, N. L., & Hibbs, M. L. (2020). Links Between Inflammatory
1053 Bowel Disease and Chronic Obstructive Pulmonary Disease. *Front Immunol*, 11, 2144.
1054 <https://doi.org/10.3389/fimmu.2020.02144>

1055 Rera, M., Bahadorani, S., Cho, J., Koehler, C. L., Ulgherait, M., Hur, J. H., Ansari, W. S., Lo, T.,
1056 Jr., Jones, D. L., & Walker, D. W. (2011). Modulation of longevity and tissue homeostasis
1057 by the *Drosophila* PGC-1 homolog. *Cell Metab*, 14(5), 623-634.
1058 <https://doi.org/10.1016/j.cmet.2011.09.013>

1059 Rera, M., Clark, R. I., & Walker, D. W. (2012). Intestinal barrier dysfunction links metabolic and
1060 inflammatory markers of aging to death in *Drosophila*. *Proc Natl Acad Sci U S A*, 109(52),
1061 21528-21533. <https://doi.org/10.1073/pnas.1215849110>

1062 Rodgers, F. H., Gendrin, M., Wyer, C. A. S., & Christophides, G. K. (2017). Microbiota-induced
1063 peritrophic matrix regulates midgut homeostasis and prevents systemic infection of
1064 malaria vector mosquitoes. *PLoS Pathog*, 13(5), e1006391.
1065 <https://doi.org/10.1371/journal.ppat.1006391>

1066 Routhier, J., Pons, S., Freidja, M. L., Dalstein, V., Cutrona, J., Jonquet, A., Lalun, N., Merol, J. C.,
1067 Lathrop, M., Stitzel, J. A., Kervoaze, G., Pichavant, M., Gosset, P., Tournier, J. M.,
1068 Birembaut, P., Dormoy, V., & Maskos, U. (2021). An innate contribution of human nicotinic
1069 receptor polymorphisms to COPD-like lesions. *Nat Commun*, 12(1), 6384.
1070 <https://doi.org/10.1038/s41467-021-26637-6>

1071 Sakornsakolpat, P., Prokopenko, D., Lamontagne, M., Reeve, N. F., Guyatt, A. L., Jackson, V.
1072 E., Shrine, N., Qiao, D., Bartz, T. M., Kim, D. K., Lee, M. K., Latourelle, J. C., Li, X.,
1073 Morrow, J. D., Obeidat, M., Wyss, A. B., Bakke, P., Barr, R. G., Beaty, T. H., . . . Cho, M.
1074 H. (2019). Genetic landscape of chronic obstructive pulmonary disease identifies
1075 heterogeneous cell-type and phenotype associations. *Nat Genet*, 51(3), 494-505.
1076 <https://doi.org/10.1038/s41588-018-0342-2>

1077 Schindelin, J., Arganda-Carreras, I., Frise, E., Kaynig, V., Longair, M., Pietzsch, T., Preibisch, S.,
1078 Rueden, C., Saalfeld, S., Schmid, B., Tinevez, J. Y., White, D. J., Hartenstein, V., Eliceiri,
1079 K., Tomancak, P., & Cardona, A. (2012). Fiji: an open-source platform for biological-image
1080 analysis. *Nat Methods*, 9(7), 676-682. <https://doi.org/10.1038/nmeth.2019>

1081 Sell, E. A., Ortiz-Carpena, J. F., Herbert, D. R., & Cohen, N. A. (2021). Tuft cells in the
1082 pathogenesis of chronic rhinosinusitis with nasal polyps and asthma. *Ann Allergy Asthma
1083 Immunol*, 126(2), 143-151. <https://doi.org/10.1016/j.anai.2020.10.011>

1084 Siedlinski, M., Tingley, D., Lipman, P. J., Cho, M. H., Litonjua, A. A., Sparrow, D., Bakke, P.,
1085 Gulsvik, A., Lomas, D. A., Anderson, W., Kong, X., Rennard, S. I., Beaty, T. H., Hokanson,
1086 J. E., Crapo, J. D., Lange, C., & Silverman, E. K. (2013). Dissecting direct and indirect
1087 genetic effects on chronic obstructive pulmonary disease (COPD) susceptibility. *Hum*
1088 *Genet*, 132(4), 431-441. <https://doi.org/10.1007/s00439-012-1262-3>

1089 Singari, S., Javeed, N., Tardi, N. J., Marada, S., Carlson, J. C., Kirk, S., Thorn, J. M., & Edwards,
1090 K. A. (2014). Inducible protein traps with dominant phenotypes for functional analysis of
1091 the *Drosophila* genome. *Genetics*, 196(1), 91-105.
1092 <https://doi.org/10.1534/genetics.113.157529>

1093 Slot, J. W., & Geuze, H. J. (2007). Cryosectioning and immunolabeling. *Nat Protoc*, 2(10), 2480-
1094 2491. <https://doi.org/10.1038/nprot.2007.365>

1095 Sone, M., Zeng, X., Larese, J., & Ryoo, H. D. (2013). A modified UPR stress sensing system
1096 reveals a novel tissue distribution of IRE1/XBP1 activity during normal *Drosophila*
1097 development. *Cell Stress Chaperones*, 18(3), 307-319. <https://doi.org/10.1007/s12192-012-0383-x>

1099 Taylor P., B. J. (1999). Synthesis, Storage and Release of Acetylcholine. In A. B. Siegel GJ,
1100 Albers RW, et al., editors (Ed.), *Basic Neurochemistry: Molecular, Cellular and Medical*
1101 *Aspects* (6th ed.). Lippincott-Raven. <https://www.ncbi.nlm.nih.gov/books/NBK28051/>

1102 Wessler, I., & Kirkpatrick, C. J. (2008). Acetylcholine beyond neurons: the non-neuronal
1103 cholinergic system in humans. *Br J Pharmacol*, 154(8), 1558-1571.
1104 <https://doi.org/10.1038/bjp.2008.185>

1105 Wilk, J. B., Shrine, N. R., Loehr, L. R., Zhao, J. H., Manichaikul, A., Lopez, L. M., Smith, A. V.,
1106 Heckbert, S. R., Smolonska, J., Tang, W., Loth, D. W., Curjuric, I., Hui, J., Cho, M. H.,
1107 Latourelle, J. C., Henry, A. P., Aldrich, M., Bakke, P., Beaty, T. H., . . . Stricker, B. H.
1108 (2012). Genome-wide association studies identify CHRNA5/3 and HTR4 in the
1109 development of airflow obstruction. *Am J Respir Crit Care Med*, 186(7), 622-632.
1110 <https://doi.org/10.1164/rccm.201202-0366OC>

1111 Yoshihara, M., Adolfsen, B., Galle, K. T., & Littleton, J. T. (2005). Retrograde signaling by Syt 4
1112 induces presynaptic release and synapse-specific growth. *Science*, 310(5749), 858-863.
1113 <https://doi.org/10.1126/science.1117541>

1114 Zeng, X., & Hou, S. X. (2015). Enteroendocrine cells are generated from stem cells through a
1115 distinct progenitor in the adult *Drosophila* posterior midgut. *Development*, 142(4), 644-
1116 653. <https://doi.org/10.1242/dev.113357>

1117 Zhang, G., Bai, H., Zhang, H., Dean, C., Wu, Q., Li, J., Guariglia, S., Meng, Q., & Cai, D. (2011).
1118 Neuropeptide exocytosis involving synaptotagmin-4 and oxytocin in hypothalamic
1119 programming of body weight and energy balance. *Neuron*, 69(3), 523-535.
1120 <https://doi.org/10.1016/j.neuron.2010.12.036>

1121

Summary of Supplemental Materials

Table S1 (Related to Figure 1)

- A) List of candidate genes for genetic variants (human) associated with COPD in Hobbs et al., 2017.
- B) List of *Drosophila* genes and RNAi lines included in the screen.

Figure S1 (Related to Figure 2)

Barrier dysfunction assays after nAChR subunit or ChAT depletion using ubiquitous or enterocyte drivers.

Figure S2 (Related to Figure 4)

Gene expression analysis after nAChR subunit depletion in enterocytes or ChAT depletion in EEs.

Figure S3 (Related to Figure 5)

Control of Peritrophic Matrix integrity by NAcHR.

Figure S4 (Related to Figure 6)

Control of Peritrophic Matrix integrity and intestinal homeostasis by Syt4.

Supplemental Materials

Table S1 (Related to Figure 1)

A) List of candidate genes for genetic variants (human) associated with COPD in Hobbs et al., 2017. Genes highlighted in blue had a clear *Drosophila* ortholog and were included in the screen.

Abbreviations used: SNP, Single nucleotide polymorphism; CHR, chromosome; BP, base pair (GRCh37); eqtl, expression quantitative trait loci; Risk allele, allele associated with increased COPD risk; Alt allele, alternative allele; OR stage1, Odds-ratio of risk allele in stage 1 of Hobbs et al., 2017; P.stage1, P-value in stage 1 of Hobbs et al; P.meta, meta-analysis P-value in Hobbs et al; Evidence.Sakornsakolpat, evidence (if available) from Sakornsakolpat et al., 2019 (GREx-genetically regulated expression, mQTL-methylation quantitative trait loci, Cod-coding association, Hi-C-chromatin interaction in human lung or IMR90 cell line, DHS-DNase hypersensitivity sites, GSet-genes identified by DEPICT, further details are available in the original publication); colocalization, probability shared causal variant between eQTL (GTEx) and COPD risk association (tissue: probability), only colocalization probability > 0.6 are listed.

B) List of *Drosophila* genes and RNAi lines included in the screen. RNAi lines were ranked according to the natural logarithm of the ratio between the proportion of smurfs after candidate gene knockdown and luciferase RNAi control. Cutoff scale shown in Fig 1C was used to determine the effect of each RNAi. Based on this fine-grained ranking of individual RNAi lines, an overall rating was assigned to each gene and compared to human eqtl data (see also Fig 1A). Temperature column refers to the temperature the subsets of RNAi lines were screened at.

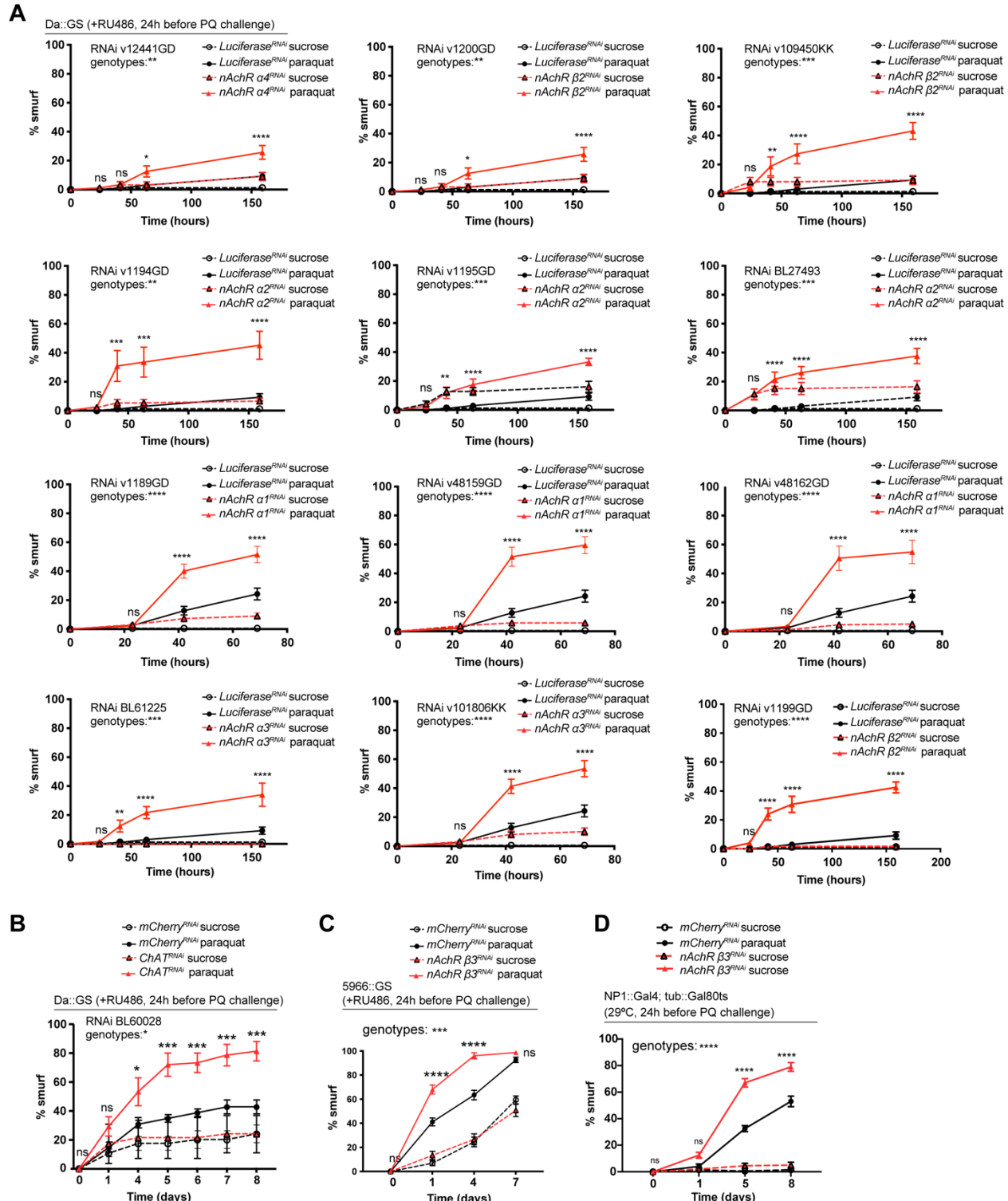


Figure S1 (Related to Figure 2)

A) Barrier dysfunction assay after mCherry (control) or indicated nAchR subunit depletion for 24h with ubiquitous driver Da::GS. N=1.

nAchR α 4 (v12441GD): n=100 for Luciferase RNAi (control) on sucrose; n=125 animals for Luciferase RNAi on sucrose+paraquat; n=125 for nAchR α 4 RNAi on sucrose; n=150 animals for nAchR α 4 RNAi on sucrose+paraquat.

nAchR β 2(v1200GD): n=100 for Luciferase RNAi (control) on sucrose; n=125 animals for Luciferase RNAi on sucrose+paraquat; n=75 for nAchR β 2 RNAi on sucrose; n=150 animals for nAchR β 2 RNAi on sucrose+paraquat

nAchR β 2(v109450KK): n=100 for Luciferase RNAi (control) on sucrose; n=125 animals for Luciferase RNAi on sucrose+paraquat; n=125 for nAchR β 2 RNAi on sucrose; n=150 animals for nAchR β 2 RNAi on sucrose+paraquat

nAchR α 2 (v1194GD): n=100 for Luciferase RNAi (control) on sucrose; n=125 animals for Luciferase RNAi on sucrose+paraquat; n=125 for nAchR α 2 RNAi on sucrose; n=150 animals for nAchR α 2 RNAi on sucrose+paraquat.

nAchR α 2 (v1195GD): n=100 for Luciferase RNAi (control) on sucrose; n=125 animals for Luciferase RNAi on sucrose+paraquat; n=125 for nAchR α 2 RNAi on sucrose; n=150 animals for nAchR α 2 RNAi on sucrose+paraquat.

nAchR α 2 (BL27493): n=100 for Luciferase RNAi (control) on sucrose; n=125 animals for Luciferase RNAi on sucrose+paraquat; n=125 for nAchR α 2 RNAi on sucrose; n=125 animals for nAchR α 2 RNAi on sucrose+paraquat.

nAchR α 1 (v1189GD): n=175 for Luciferase RNAi (control) on sucrose; n=175 animals for Luciferase RNAi on sucrose+paraquat; n=175 for nAchR α 1 RNAi on sucrose; n=175 animals for nAchR α 1 RNAi on sucrose+paraquat.

nAchR α 1 (v48159GD): n=150 for Luciferase RNAi (control) on sucrose; n=150 animals for Luciferase RNAi on sucrose+paraquat; n=125 for nAchR α 1 RNAi on sucrose; n=150 animals for nAchR α 1 RNAi on sucrose+paraquat.

nAchR α 1 (v48162GD): n=1075 for Luciferase RNAi (control) on sucrose; n=175 animals for Luciferase RNAi on sucrose+paraquat; n=150 for nAchR α 1 RNAi on sucrose; n=150 animals for nAchR α 1 RNAi on sucrose+paraquat.

nAchR α 3 (BL61225): n=100 for Luciferase RNAi (control) on sucrose; n=125 animals for Luciferase RNAi on sucrose+paraquat; n=50 for nAchR α 3 RNAi on sucrose; n=75 animals for nAchR α 3 RNAi on sucrose+paraquat.

nAchR α 3 (v101806KK): n=175 for Luciferase RNAi (control) on sucrose; n=175 animals for Luciferase RNAi on sucrose+paraquat; n=175 for nAchR α 3 RNAi on sucrose; n=175 animals for nAchR α 3 RNAi on sucrose+paraquat.

nAchR β 2: n=100 for Luciferase RNAi (control) on sucrose; n=125 animals for Luciferase RNAi on sucrose+paraquat; n=75 for nAchR β 2 RNAi on sucrose; n=100 animals for nAchR β 2 RNAi on sucrose+paraquat.

B) Barrier dysfunction assay after mCherry (control) or ChAT depletion for 24h with ubiquitous driver Da::GS. n=60 animals per genotype and condition; N=3. Two-way ANOVA followed by Šídák's multiple comparisons test.

C) Barrier dysfunction assay after mCherry (control) or nAchR β 3 depletion for 24h with enterocyte-specific driver 5966::GS. nAchR β 3: n=175 for mCherry RNAi (control) on sucrose;

n=175 animals for mCherry RNAi on sucrose+paraquat; n=150 for nAchR β 3 RNAi on sucrose; n=150 animals for nAchR β 3 RNAi on sucrose+paraquat. N=3. Two-way ANOVA followed by Šídák's multiple comparisons test.

D) Barrier dysfunction assay after mCherry (control) or nAchR β 3 depletion for 24h with enterocyte-specific driver NP1::Gal4, tub::Gal80^{ts} (NP1^{ts}). n=200 animals per genotype and condition; N=3. Two-way ANOVA followed by Šídák's multiple comparisons test.

Data presented as mean \pm SEM. ns, not significant, P > 0.05; *P \leq 0.05; **P \leq 0.01; ***P \leq 0.001; ****P \leq 0.0001. n: number of animals or midguts analyzed; N: number of independent experiments performed with similar results and a similar n

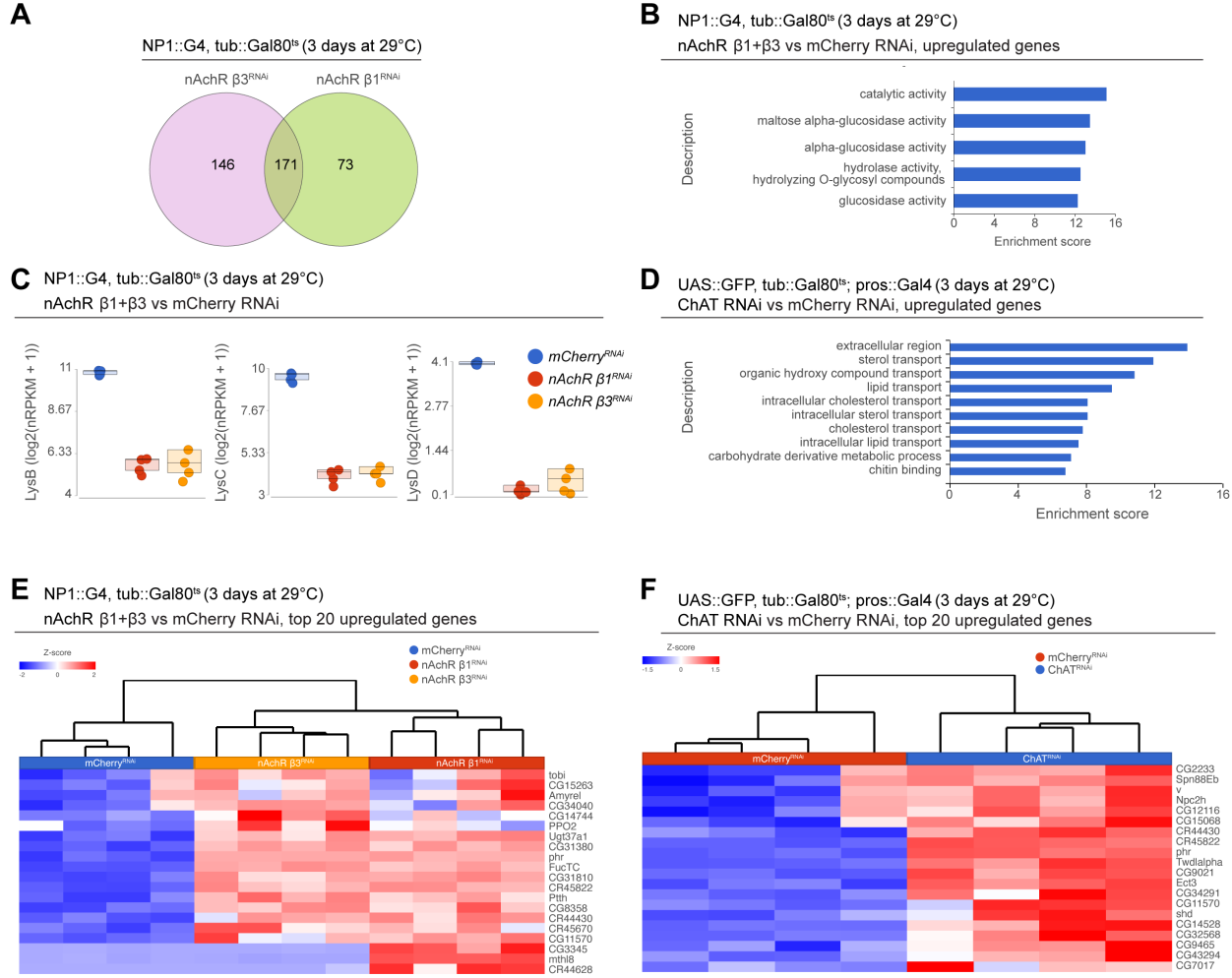


Figure S2 (Related to Figure 4)

- A) Overlap between differentially regulated genes after 3 days of nAChR $\beta 1$ or $\beta 3$ depletion in enterocytes with NP1^{ts}.
- B) GO term enrichment of significantly upregulated genes after 3 days of nAChR $\beta 1$ and $\beta 3$ knockdown with NP1^{ts}.
- C) Transcript levels of lysozyme family members in bulk RNAseq data set after 3 days of mCherry (control) or nAChR $\beta 1$ and $\beta 3$ subunit depletion in ECs.
- D) Gene set enrichment analysis of significantly upregulated genes after ChAT depletion in EEs.
- E) Heatmap of the top 20 upregulated differentially expressed genes after nAChR $\beta 1$ and $\beta 3$ knockdown in ECs for 3 days. (FDR ≤ 0.1 ; $\log_2(\text{fold change}) > 2.5$; 100% of samples have ≥ 1 reads)
- F) Heatmap of top 20 upregulated differentially expressed genes after 3 days of ChAT depletion with RNAi in EEs under control of pros^{ts}. (FDR ≤ 0.1 ; $\log_2(\text{fold change}) > 1.97$; 100% of samples have ≥ 1 reads)

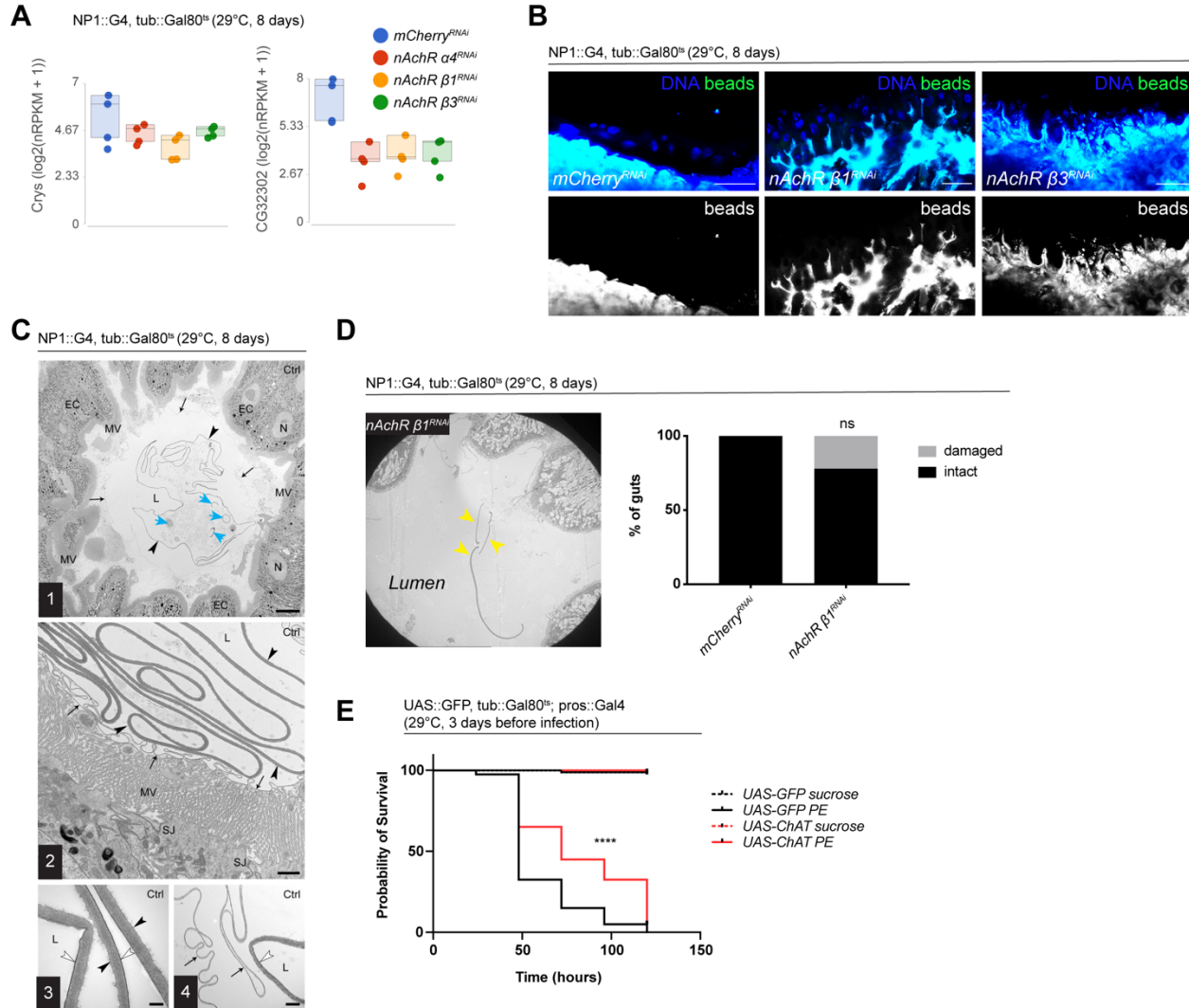


Figure S3 (Related to Figure 5)

A) Transcript levels of two PM components in bulk RNAseq data set after 8 days of mCherry (control) or nAchR subunit depletion in ECs.

B) Confocal immunofluorescence image of posterior midguts depleted for either mCherry (control), nAchR $\beta 1$ or $\beta 3$ for 8 days. Animals were fed green fluorescent beads to assess Peritrophic matrix (PM) integrity. DNA (blue) is labeled with Hoechst. n=10 guts. N=3. Scale bar 25 μ m.

C) Overview of PM layers in posterior midgut (R4) of control animals. (1) The PM lies as an intact ring (black arrowheads) loosely in the gut lumen surrounded by an additional thin layer ring (small arrows). The PM encloses food remnants and short segments of material with a similar ultrastructure as the PM (blue arrows). (2) Detail of the PM layers: Thick layer (black arrowheads) and thin layer ring (small arrows) on top of microvilli of the enterocytes. Septate junctions (SJ) seal the intercellular spaces between the enterocytes at their apical edges. (3) Detail of the PM ultrastructure. The luminal surface (white arrowhead) is lined by an electron-dense layer of

constant thickness. The abluminal surface is less electron-dense and slightly rough (black arrowheads). (4) Detail of the thin layer ring (black arrows)

L, gut lumen. EC, enterocyte. MV, microvilli. N, nucleus. Scale bars: 10 μ m (1), 1 μ m (2), 200 nm (3), 500 nm (4).

D) Example image of damaged thick PM layer, yellow arrowheads highlight PM fragments in the gut lumen. Quantification of thick PM layer integrity after 8 days of mCherry (control) or nAchR β 1 knockdown in ECs. n=16; 18 midguts for mCherry or nAchR β 1, respectively. N=1. Fisher's exact test.

E) Survival after 3 days of mCherry (ctrl) or ChAT overexpression in EEs followed by *Pseudomonas entomophila* infection. n=80 animals for UAS-GFP on sucrose or sucrose+PE; n=40 animals for UAS-ChAT on sucrose or sucrose+PE; N=3. Log Rank (Mantel-Cox) test.

Data presented as mean \pm SEM. ns, not significant, P > 0.05; *P \leq 0.05; **P \leq 0.01; ***P \leq 0.001; ****P \leq 0.0001. n: number of animals or midguts analyzed; N: number of independent experiments performed with similar results and a similar n.

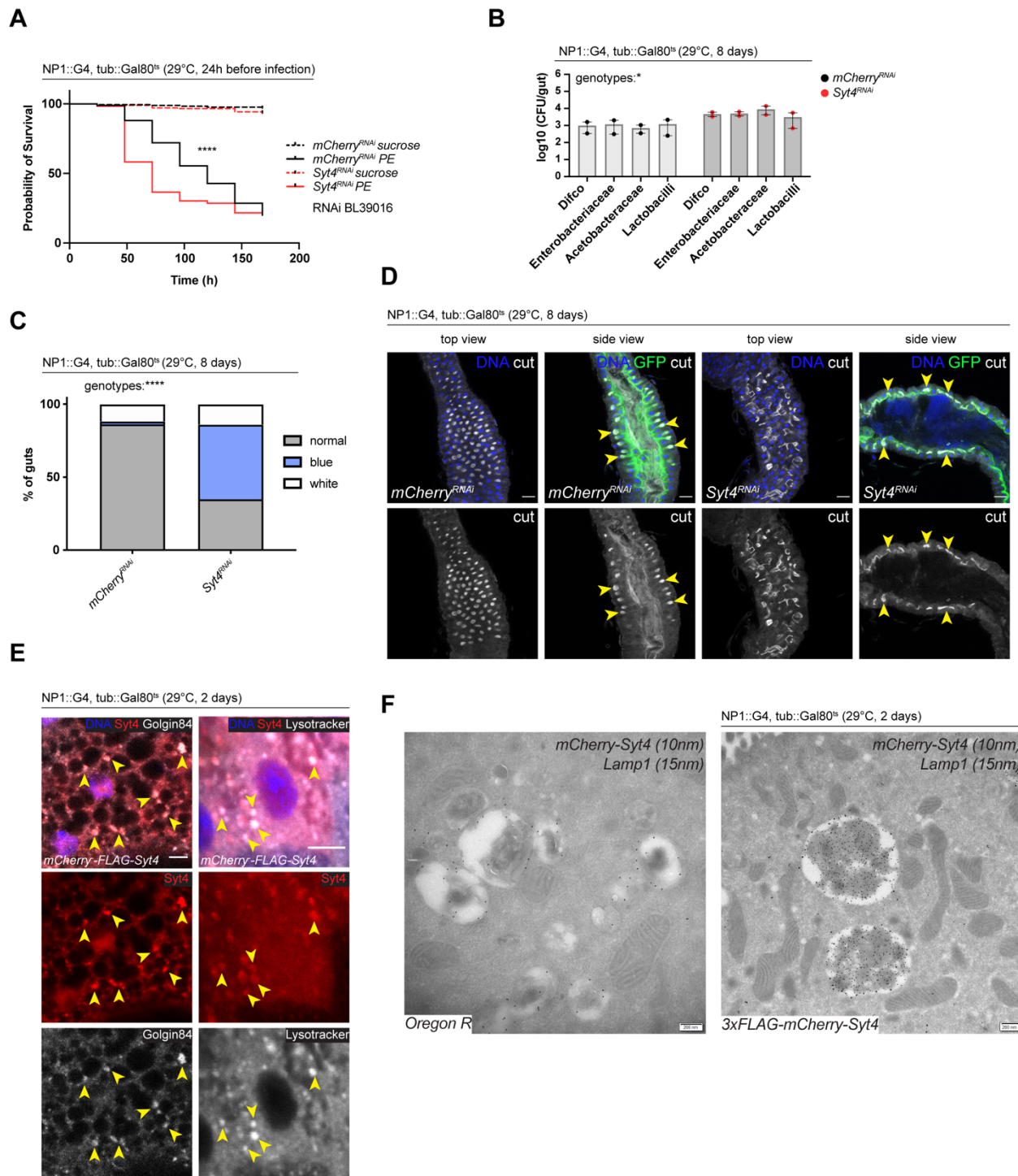


Figure S4 (Related to Figure 6)

A) Survival after one day of mCherry (ctrl) or Syt4 depletion in ECs followed by *Pseudomonas entomophila* infection. n=175 animals per genotype and condition; N=3. Log Rank (Mantel-Cox) test.

B) CFU of whole guts plated on selective growth media after 8 days of Syt4 depletion in ECs. 2 pooled independent experiments are shown. n=5 pooled animals per genotype and experiment. Two-way ANOVA.

C) Analysis of gut compartmentalization visualized by feeding Bromphenol blue pH indicator (see Fig 5E) after 8 days of Syt4 knockdown in ECs. n=51 guts for mCherry (control), n=43 guts for Syt4 RNAi. 3 independent pooled experiments are shown. Chi square test.

D) Confocal immunofluorescence images of posterior midguts depleted of either mCherry (control) or Syt4 in enterocytes for 8 days, stained with anti-cut antibody (white). Guts are expressing a GFP-brush border marker (green). DNA (blue) is labeled with Hoechst. Yellow arrowheads in side view panels highlight healthy, pocket-like (mCherry) and disrupted gastric units (Syt4-RNAi). n=10 guts. N=3. Scale bar 25 μ m.

E) Confocal immunofluorescence image of posterior midguts overexpressing UAS-FLAG-mCherry-Syt4 (red) in enterocytes stained with anti-Golgin84 antibody or Lysotracker (white). DNA (blue) is labeled with Hoechst. Yellow arrowheads indicate overlap between Syt4-positive vesicles and Golgin84 or Lysotracker staining. n=10 guts. N=3. Scale bar 5 μ m.

F) Immunogold electron microscopy image of Syt4 and Lamp1 co-staining in enterocytes of posterior midguts of either wildtype Oregon R flies or animals expressing UAS-FLAG-mCherry-Syt4 under control of NP1ts. Syt4 (detected with mCherry antibody 10nm gold particles) and Lamp1 (15nm gold particles) are colocalizing on multilamellar bodies in animals expressing the Syt4 construct. Oregon R samples are devoid of anti-mCherry antibody staining. n=5 guts. N=1. Scale bar 200nm.

Data presented as mean \pm SEM. ns, not significant, P > 0.05; *P \leq 0.05; **P \leq 0.01; ***P \leq 0.001; ****P \leq 0.0001. n: number of animals or midguts analyzed; N: number of independent experiments performed with similar results and a similar n.